

DECIPHERING THE BIOCHEMICAL INTERACTIONS OF THE
MECHANORESPONSIVE CONTRACTILITY CONTROLLER

by
Priyanka Kothari

A dissertation submitted to Johns Hopkins University in conformity with the
requirements for the degree of Doctor of Philosophy

Baltimore, Maryland
January 2020

Abstract

Every biological process, ranging from cell migration to embryogenesis, relies on the cell's ability to adapt to changing mechanical environments. Cellular contractility is governed by a control system of proteins that integrates internal and external cues to drive diverse shape change processes. This contractility controller includes myosin II motors, actin crosslinkers, and protein scaffolds, which exhibit robust and cooperative mechanoaccumulation. However, the biochemical interactions and feedback mechanisms that drive the controller remain unknown. Here, we use a proteomics approach to identify direct interactors of two key nodes of the contractility controller in the social amoeba *Dictyostelium discoideum*: the actin crosslinker cortexillin I and the scaffolding protein IQGAP2. We highlight several unexpected proteins that suggest feedback from metabolic and RNA-binding proteins on the contractility controller. Quantitative *in vivo* biochemical measurements reveal interactions between myosin II and cortexillin I, which form the core mechanosensor. Further, IQGAP1 negatively regulates mechanoresponsiveness by competing with IQGAP2 for binding the myosin II-cortexillin I complex. These myosin II-cortexillin I-IQGAP2 complexes are pre-assembled into higher order mechanoresponsive contractility kits (MCKs) poised to integrate into the cortex upon diffusional encounter coincident with mechanical inputs.

Primary Reader and Advisor: Douglas N. Robinson, Ph.D.

Secondary Reader: Pablo A. Iglesias, Ph.D.

Acknowledgements

I would first like to thank Doug for his incredible mentorship. Doug has not only taught me about mechanobiology, but has also taught me how to think critically about a problem and create detailed, testable hypotheses to answer it. He allowed me to explore the science that interested me, bring in new methods when available, and provided guidance where needed. His constant encouragement and advice, whether it was science, career, or even house-related, was always appreciated. The fact that I can now only read documents that are in Arial font should also be credited to Doug.

I have also always been surrounded by amazing mentors and colleagues that inspire me every day. I want to thank my 7th grade science teacher, Mr. Coe, whose enthusiasm and passion initially piqued my curiosity in cell and molecular biology. I would also like to thank the members of my thesis committee, Pablo Iglesias, Rong Li, and Jie Xiao, for their great scientific insight, career advice, and support throughout my graduate career. A special thank you to Alexandra Surcel, for being a strong female mentor when I did not realize I needed one. Thank you to all the folks in the Robinson lab (past and present) who challenged me to think more critically and made working in the lab so entertaining and enjoyable. Thank you to my BCMB classmates and in particular, my friends Meiling and Michelle for making grad school so much fun.

I would also like to thank Adam Hancock, who always encouraged and believed in me even when I did not believe I could accomplish something myself. He taught me to manage my time and set specific goals, and has also made me realize the important things in life, which has made this journey even more enjoyable. Thank you to my sister, Ruchita, for always being cheerful and fun to be around, and for her caring support. It has been

wonderful seeing her grow over the past few years, both as a friend and even a fellow collaborator.

Finally, I will forever be grateful for my parents, Anita and Subhash Kothari, for their unconditional love and support over the years as I pursued my passion for science. Thank you for always believing in me and constantly encouraging me to be the best version of myself.

Table of Contents

Abstract	ii
Acknowledgements	iii
List of Tables	vi
List of Figures	vii
Chapter 1 Introduction	1
Control systems	3
Establishing the setpoint	7
Force-sharing.....	9
Feedback across long-time scales	12
Chapter 2 Materials and Methods	17
Reagents	17
Cell strains and Culture.....	18
Anti-FLAG Co-immunoprecipitation.....	21
Single-Molecule Pull-down (SiMPull).....	21
Fluorescence Correlation Spectroscopy (FCS)	23
Fluorescence Recovery after Photobleaching	31
Agarose Overlay	32
Statistics	32
Chapter 3 Using FCCS to measure <i>in vivo</i> binding affinities	34
Chapter 4 Contractility kits promote assembly of the mechanoresponsive cytoskeletal network	36
Identification of direct, biochemical interactions within the mechanobiome.....	38
Cortexillin I and IQGAP2 interact with myosin II <i>in vivo</i>	40
Regulatory proteins also interact with the contractility controller.....	46
IQGAP1 inhibits the interaction between cortexillin I and IQGAP2	48
Quantifying the stoichiometries of core building blocks	50
Chapter 5 Uncovering the role of mmsdh in the contractility controller	58
Chapter 6 Conclusions	61
Chapter 7 Future Directions	67
Contributions	70
Bibliography	71
Curriculum Vitae	81

List of Tables

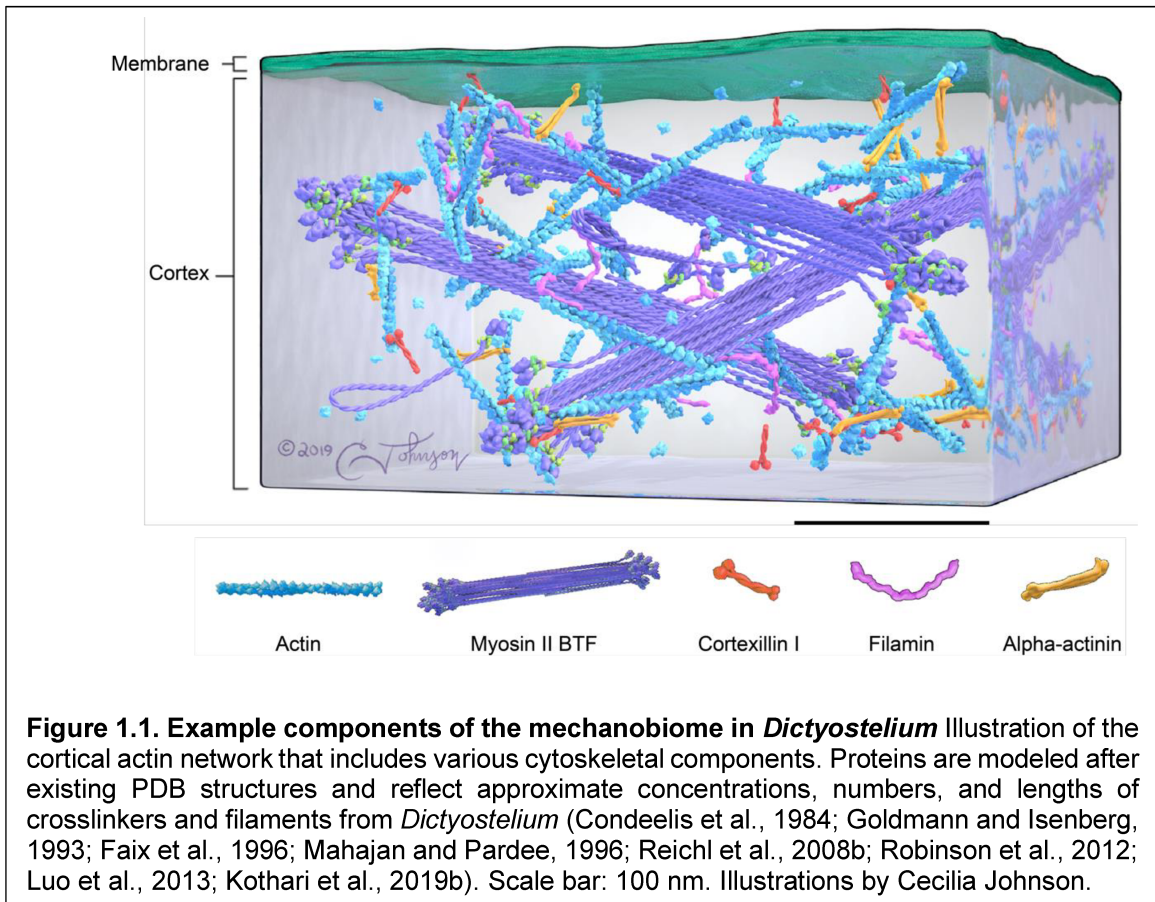
Table 1. List of Dictyostelium strains used.	20
Table 2: Concentrations and <i>in vivo</i> K_D 's by FCCS.....	55

List of Figures

Figure 1.1. Example components of the mechanobiome in <i>Dictyostelium</i>	1
Figure 1.2. Control systems and setpoint theory	8
Figure 2.1. Single-Molecule Pull-down to assess complex stoichiometry	22
Figure 2.2. Fluorescence Correlation Spectroscopy to assess protein dynamics in live cells	25
Figure 3.1. FCCS in <i>myoII</i> -null <i>Dictyostelium</i> cells to measure apparent binding affinities between myosin II and 14-3-3.....	34
Figure 4.1. Identification of protein interactors of the contractility control system by mass spectrometry and immunoprecipitation	37
Figure 4.2. Cortexillin I and IQGAP2 interact with myosin II in the cytoplasm as detected by Fluorescence Cross-Correlation Spectroscopy (FCCS).....	42
Figure 4.3 No correlation is detected between protein concentration and <i>in vivo</i> K_D	43
Figure 4.4. Correlation times of myosin II, cortexillin I, and IQGAP2, and <i>in vivo</i> K_D 's of IQGAP1 with myosin II and cortexillin I	45
Figure 4.5. Apparent <i>in vivo</i> K_D 's measured for interactions from proteomics.....	47
Figure 4.6. IQGAP1 inhibits the IQGAP2-cortexillin I interaction	49
Figure 4.7. Interaction between IQGAP2 and cortexillin I is unaffected by Lat A treatment.....	50
Figure 4.8. Single-molecule images demonstrate colocalization of cortexillin I with IQGAP1 and IQGAP2	53
Figure 4.9. IQGAP1 and IQGAP2 bind cortexillin I with different stoichiometries ..	54
Figure 5.1. Dynamics of GFP-3xAsp myosin II in the presence of <i>mmsdh</i>	59
Figure 5.2 <i>Mmsdh</i> overexpression alters cortical accumulation of an assembly-deficient myosin II upon mechanical stress	60
Figure 6.1. The network of biochemical interactions in the contractility controller	62

Chapter 1 Introduction

Control over cell shape changes is vital for processes ranging from cytokinesis and cell migration to more complex events, such as tissue development and homeostasis, wound healing, and immune function. Cells have evolved to respond to mechanical stimuli, including stretch, compression, and shear forces, as well as internally generated tension and strain. We define the mechanobiome as the set of macromolecules that allows cells to generate, sense, and respond to such forces (Kothari et al., 2019b; Surcel and Robinson, 2019). The mechanobiome incorporates many components of the cytoskeleton, including myosin II motor proteins, actin crosslinkers, scaffolding proteins, actin polymerization and depolymerization factors, small GTPases, and other cytoskeletal polymer systems (Wu et al., 2008; Robinson et al., 2012; Blanchoin et al., 2014; Zaidel-



Bar et al., 2015; Chugh and Paluch, 2018; Dogterom and Koenderink, 2019). This term includes components that build cell-cell and cell-matrix interactions (“adhesome”), as well as all the proteins and networks commonly included in the “contractome” (Zaidel-Bar et al., 2015; Horton et al., 2016). The benefit of the larger umbrella term “mechanobiome” is that it recognizes that each of these seemingly discrete systems are integrated with one another. In addition, although actin, microtubule, and intermediate filament networks have often been considered independently, these networks really work synergistically to drive cellular processes (Zhou et al., 2010; Huber et al., 2015; Henty-Ridilla et al., 2016; Dogterom and Koenderink, 2019).

The cell cortex is an approximately 200-500-nm thick composite material that includes the plasma membrane and the dense actin meshwork that lies just below the membrane (**Fig. 1.1**) (Reichl et al., 2008a; Robinson et al., 2012; Clark et al., 2013). Along with the underlying and penetrating cytoplasm, the cell cortex contributes to the mechanical properties of a cell. Cells are active viscoelastic fluids and the collection of mechanical stresses at the cell cortex leads to a cortical (surface) tension that serves to minimize the ratio between surface area and volume of the cell, in essence a rounding pressure (Robinson et al., 2012; Moeendarbary and Harris, 2014). The membrane itself constitutes an upper limit of approximately 2-5% of the total cortical tension value (Luo et al., 2014). The remaining active and passive portions of cortical tension are largely generated by the cytoskeletal network. These networks are viscoelastic in nature, allowing for time-scale dependent behaviors in response to mechanical stresses (Gardel et al., 2004; Robinson et al., 2012; Pegoraro et al., 2017; Chugh and Paluch, 2018). The elastic component is derived from the strong interactions between actin filaments and crosslinkers that build the cytoskeletal meshwork, whereas the viscous component is a result of those structures remodeling over time to relieve the stress imposed on the system.

Here, I focus on the biochemical interactions and feedback mechanisms that regulate the cytoskeletal network primarily at the cellular level. Specifically, I discuss the application of theoretical principles from control engineering to cellular systems to understand how the actomyosin network influences cell behaviors. Cells integrate biochemical and mechanical inputs through the use of control systems that rely on sensors, actuators, and feedback loops. Examples of control systems in the context of the actin cytoskeletal network demonstrate mechanisms that regulate the setpoint (baseline) through differential protein-binding affinities, post-translational modifications, force-sharing across a network, and complex assemblies. Additionally, we explore how seemingly unrelated processes (e.g. gene regulation, metabolism, and cell fate determination) and cell mechanics feedback onto each other to orchestrate complex cellular events. I primarily use myosin II as an example of a protein that functions both as a sensor and actuator in the context of setpoint and feedback. However, these concepts also apply more broadly to many other components of the mechanobiome as well. The application of control theory principles will provide systems-level insight into how cells respond to the forces they encounter during normal and disease-state processes. It is worth noting that the mechanics of cell-cell junctions, cell-extracellular matrix, and tissues have been recently reviewed elsewhere (Charras and Yap, 2018; Chen et al., 2018; Yap et al., 2018; Sun et al., 2019).

Control systems

To ensure robust cellular mechanical behaviors, the cytoskeletal network functions as a control system, which includes sensors to detect environmental cues or deviations away from a desired behavior, and actuators, which execute the desired behavior or process (**Fig. 1.2A**) (Ren et al., 2009; Kee et al., 2012; Srivastava and Robinson, 2015; Srivastava et al., 2016; Schiffhauer and Robinson, 2017; Schiffhauer et al., 2019). Inherently, control

systems may be open- or close-looped. In the open-loop scenario, the actuator response is based on sensed changes to an input. In the closed-loop situation, the system monitors the progress of the desired behavior or process and makes adjustments, thus closing positive and/or negative feedback loops. The system behavior is measured against an adjustable setpoint, which establishes the reference point that the system uses to define baseline (**Fig. 1.2B**). By regulating the setpoint, each individual system is poised to respond differently to disturbances. All components, sensors, actuators, feedbacks, and setpoints are tunable.

In the cell, macromolecules such as receptor proteins, small GTPases, metabolites, and mechanoresponsive proteins (proteins that sense and accumulate in response to a local mechanical stress) function as sensors, receiving biochemical and mechanical inputs and signaling to actuators. In many cases, proteins in a control system function as both sensors and actuators, allowing the cell to use the same system that generates the foundational mechanical properties to also adapt to constantly changing inputs. For instance, the force-sensing, actin-binding cooperativity, and corresponding allostery in the actin filament allow myosin II to sense and respond to load (force) in the actin network, thus functioning as both a sensor and actuator (Galkin et al., 2012; Kee et al., 2012; Luo et al., 2012). Mechanoresponsive actin crosslinkers, such as alpha-actinin and filamin, also provide a similar functionality as well (Luo et al., 2013; Schiffhauer et al., 2016; Schiffhauer and Robinson, 2017).

One example for the action of a control system may be observed during cleavage furrow ingression, which is a critical step in ensuring genomic fidelity and therefore needs to be an incredibly robust process with the ability to adapt to a dynamic environment. Thus, relying on a control system that integrates many inputs and implements feedback would be advantageous. In fact, in *Dictyostelium*, cleavage furrow assembly is driven by the cellular contractility control system, which can be described in a few components: the

cytokinetic signaling module (signal input), the plant, which includes the contractile machinery (myosin II and actin crosslinker cortexillin I, which are the sensors and actuators), and feedback loops constructed in part by IQGAP regulatory proteins (**Fig. 1.2 A,C**) (Kee et al., 2012; Srivastava and Robinson, 2015). The cell must transition from its default setting of resisting shape change to coordinating a major shape-change event, thus requiring differential sensitivities, or thresholds, to mechanical stresses. First, the system has a setpoint that is tuned and varies across the cell cycle. Second, through feedback in response to internally- or externally-generated stress, the system tunes the amount of contractile proteins that accumulates at the cleavage furrow cortex, ensuring robustness.

Initially, the cytokinetic signaling module built from a kinesin 6 protein (Kif12 in *Dictyostelium*) and inner centromere protein (INCENP) provides the initial input that leads to recruitment of contractile proteins. The associated shift in setpoint is demonstrated by the changes in the amount of force that is required to elicit a myosin II mechanoresponse over the cell cycle. During anaphase, the system becomes extremely sensitive to mechanical stress, and low forces are sufficient to induce a myosin II mechanoresponse (Efler et al., 2006; Ren et al., 2009). However, the same magnitude of response requires a significantly higher force (~2.5-fold) during interphase and the early phases of mitosis. In fact, a metaphase cell can be clamped with a micropipette used to apply a defined amount of mechanical stress, and the myosin II will not undergo mechanoresponsive accumulation (mechanoaccumulation) until the cell enters anaphase. This setpoint appears to be established by the RacE small GTPase, as null mutants of *racE* require only low mechanical stresses throughout the cell cycle to trigger myosin II mechanoaccumulation. As RacE maintains certain actin crosslinkers (dynacortin), as well as regulators of myosin II (14-3-3 proteins), on the cortex, this mutant identifies two mechanisms for modulating setpoint control: force sharing and myosin II assembly

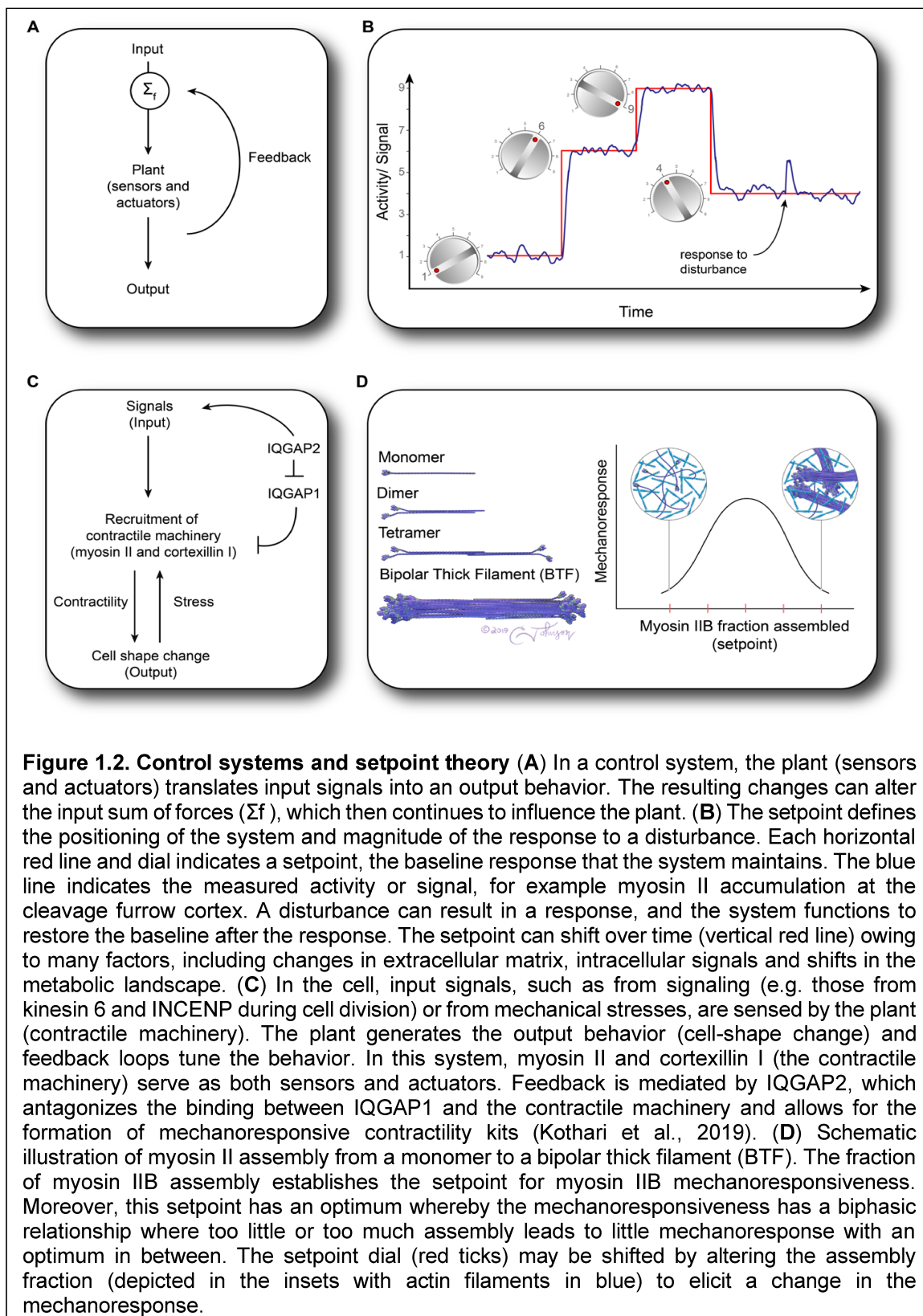
regulation (see below) (Robinson and Spudich, 2000; Zhou et al., 2010; West-Foyle et al., 2018).

Using theoretical concepts from control engineering, we could explain the biphasic nature of the mechanosensory response of cells (Luo et al., 2013; Mohan et al., 2015). Myosin II accumulation is biphasic, first accumulating to resist deformation, then contracting against load, and finally dissipating as the deformation is corrected. Previously, mathematical models had been used to explain the experimentally observed accumulation of contractile proteins at the site of mechanical perturbations (Luo et al., 2012). However, these models could not explain the biphasic nature of these accumulations. Incorporating the role of myosin II as a sensor and an actuator that provides force feedback was an important step in explaining the system.

The architecture of control systems is also observable in other processes involved in cell motility and tissue morphogenesis, including those driven by excitable, pattern forming, and self-organizing systems. In *Xenopus laevis*, waves of contractility regulators lead to cortical remodeling that eventually coordinates furrow formation (Bement et al., 2015). In *Dictyostelium*, the signal transduction excitable network (STEN) promotes protrusions and cytoskeletal reorganization that lead to cell migration. Decreasing the threshold, or setpoint, of STEN by synthetically decreasing the levels of phosphatidylinositol-4-5-bisphosphate alters the actin-based protrusive activity and drives transitions between distinct migratory modes (Miao et al., 2017). Similarly, the positive and negative feedback through phosphorylation and dephosphorylation cycles of the myosin light chain kinase and the resulting contractions of myosin II generate a self-organized control system that regulates the pulsatile contractions that promote tissue morphogenesis during germband extension in *Drosophila melanogaster* (Munjal et al., 2015).

Establishing the setpoint

By shifting the baseline, or setpoint, of a control system, a single cell can have different sensitivities and outputs in response to biochemical and mechanical cues (**Fig. 1.2B**). The setpoint may be established by varying protein affinities, post-translational modification states, the assembly state of the protein(s), and protein-protein interactions. For example, an optimal actin-binding affinity is required for actin crosslinkers filamin and alpha-actinin to be mechanoresponsive. If the actin-binding affinity is too low, the crosslinker is prevented from binding the network sufficiently, whereas in the case of a very high binding affinity, sufficient turnover to allow the dynamic behavior of the protein is inhibited (Schiffhauer et al., 2016). Modeling this relationship between actin-binding affinities and mechanoresponse allowed for the accurate prediction of which mammalian crosslinker isoforms would mechanorespond. Specifically, theory predicted and experiment verified that filamin B and alpha-actinin 4 mechanorespond strongly. In contrast, theory predicted that alpha-actinin 1 would not respond and filamin A would do so very weakly and over a much longer timeframe; neither protein displayed mechanoaccumulation experimentally (Schiffhauer et al., 2016). These observations suggest that the actin-binding affinity at the level of interaction between a single actin binding domain and actin helps define the mechanoresponsive ability and the kinetics of the response. By changing expression patterns of these isoforms, modulating effective affinities through post-translational modifications, or steric hindrance caused by protein-protein interactions, cells may alter their setpoints, and thus their mechanoresponsive abilities.



Setpoint control also provides insight into the functions and behaviors of different cell types. The baseline fraction of assembly of non-muscle myosin IIB into bipolar thick filaments (BTFs) predicts its mechanoresponsive ability across a wide range of cell types, including NIH 3T3 fibroblasts, HeLa, and Jurkat cells (Schiffhauer et al., 2019). The mechanism underlying this setpoint control depends upon phosphorylation of the myosin heavy chain, which serves to maintain each cell-type's particular ratio of unassembled (free) to assembled (bipolar filaments) myosin IIB subunits for each cell type. In Jurkat cells, 20% of myosin IIB is assembled and robustly mechanoresponds. 3T3 and HeLa cells, in which myosin assembly is 5% and 30%, respectively, have a poor myosin IIB mechanoresponse. As heavy chain phosphorylation inhibits myosin IIB assembly, manipulation of the Serine 1935 residue or PKC ζ kinase, which phosphorylates this residue, was sufficient to shift the systems towards the 20% myosin IIB assembly, increasing its mechanoresponse (**Fig. 1.2D**) (Schiffhauer et al., 2019). This example illustrates how protein post-translational modification, phosphorylation in this case, can be used by cells to control setpoint. In addition, the load-bearing capabilities of the structural proteins themselves can have impact at a distance, allowing force-sharing between the proteins to be another means of tuning the setpoint.

Force-sharing

The RacE-mediated tuning of myosin II mechanoresponsiveness discussed earlier suggested force-sharing as a means of controlling setpoint (Effler et al., 2006; Ren et al., 2009). Direct studies of the molecular entities that generate the foundational mechanics confirmed force-sharing as a mechanism of distribution of forces across a cytoskeletal network (Luo et al., 2013). Traditionally a phenomenon studied in engineering, the concept of force-sharing describes multiple components bearing the load of a system or network.

Because forces across the cortex are shared between the actin crosslinkers and myosin II, the more proteins across which to distribute the load, the less load each protein experiences. Furthermore, changes in the total amount of load-bearing proteins impact the amount of load experienced by the mechanoresponsive proteins, thereby affecting their ability to mechanorespond. For example, in *Dictyostelium*, the cross-linker alpha-actinin only displays mechanoresponsiveness in the absence of myosin II, suggesting that this crosslinker only experiences enough force to mechanorespond when myosin is not sharing load in the network. In addition, removal of some types of actin crosslinkers, including those which are not mechanoresponsive (e.g. dynacortin), reduces the amount of stress necessary to trigger a myosin II mechanoresponse (Luo et al., 2013). Thus, force sharing represents a systems-level determinant of setpoint positioning.

Once the forces are experienced by the crosslinkers, the actin-binding lifetime is modulated by the catch-slip characteristics of the crosslinker-actin bond. A catch-slip bond is a type of bond where low to moderate forces increase the binding lifetime and higher forces decrease binding lifetime. If the force surpasses a threshold, this decreases the binding affinity, causing the bond to fail (Chan and Odde, 2008). Thus, if load is too widely distributed across the network, individual crosslinkers may not sense sufficient load to engage. Conversely, if there are too few crosslinkers sharing the load, the force of each of them may be too great, causing the crosslinkers to slip and release from the actin. Therefore, the catch-slip-bond nature of proteins predicts the scenario of a biphasic relationship between load and the ability of a protein to engage with the network, and an “optimal” force that allows for proteins to mechanorespond.

Myosin II represents a special case where mechanical load triggers the myosin II to stall in the isometric transition state, which is also the cooperative binding state. In this state, the lifetime of binding to the actin filaments is increased and induces allosteric conformational changes along the actin filament that allows for cooperative binding of

myosin motors and localized assembly of bipolar thick filaments (Mahajan et al., 1989; Veigel et al., 2003; Ren et al., 2009; Tokuraku et al., 2009; Uyeda et al., 2011; Luo et al., 2012). This behavior allows for the tension in the cytoskeletal network to be shared across many myosin motors. These motors can then maintain tension or remodel the network, relieving the stress. In fact, differences in the actin-binding duty ratio of non-muscle myosin II molecules likely contribute to different behaviors of the mammalian myosin II isoforms. For example, the higher-duty ratio of non-muscle myosin IIB allows it to bear resistive strains over long-time scales (Kovacs et al., 2007; Nagy et al., 2013), thus allowing it to form stable structures at the rear of a migrating cell (Shutova et al., 2017).

In the context of cytokinesis, these force-sensitive properties of the crosslinkers and myosin II have unexpected consequences. Studies found that depletion of actin crosslinkers and myosin II increases the velocity of cytokinesis furrow ingression during late stages of cytokinesis, whereas their over-expression can lead to cytokinetic failure (Robinson and Spudich, 2000; Zhang and Robinson, 2005; Mukhina et al., 2007; Kee et al., 2012; Descovich et al., 2018). This behavior is due to the interface between contractility, cortical viscoelasticity, and the passive fluid mechanics of the furrow ingression process. Furthermore, as the network becomes loaded, the crosslinkers and motors bind more tightly, leading to a stiffer network (strain-stiffening mechanics) (Reichl et al., 2008a; Poirier et al., 2012; Srivastava and Robinson, 2015).

In addition, force-sharing is visible in the context of superdiffusive behaviors of the cortex. Much of the super-diffusive behaviors of the cell are lost in *Dictyostelium* cells with a myosin II heavy chain knockout (encoded by the *mhcA* gene; *myoII* null), and this super-diffusivity is not restored by an uncoupler myosin II mutant that has normal ATPase activity, but a short step size (Girard et al., 2006). These observations naturally implicate myosin II as the active component that drives fluidity. However, depletion of actin crosslinker dynacortin in the *myoII* null cells significantly restores their super-diffusive

behavior, suggesting that myosin II activity promotes the active components of the cortex, but does not necessarily generate them on its own. In fact, multiple molecular components contribute to these dynamical phenomena and cell mechanics, and in essence, one role of myosin II is to help “stir the pot”, antagonizing some of the cross-linkers and allowing these super-diffusive behaviors to emerge (Girard et al., 2006).

On a larger scale, measuring cortical flow behaviors in the *Caenorhabditis elegans* zygote has revealed the concept of morphogenetic degeneracy (Naganathan et al., 2018). Actin cortex structure and dynamics (including cortical flow velocities, chirality, and myosin II foci) were quantified upon depletion of various actin-binding proteins and actomyosin regulators. Through dimensional analysis, certain proteins that had similar effects on cortical flow could be grouped into specific phenotypes, including changes in chirality index and oscillations of cortical flow. The interpretation is that cortical mechanics are “course-grained,” allowing various components to contribute similarly to a single phenomenon, which on a molecular level may be explained by force-sharing. Force-sharing may then be a mechanism that generally provides robustness to shape change processes.

Feedback across long-time scales

Feedback through mechanoresponsive proteins can occur within time scales from a few seconds to minutes, although the associated feedback loops also function over prolonged periods of time to integrate different cellular processes. Mechanically-transduced transcription factors have emerged as key regulators of the feedback between the mechanical state of the cell and changes in gene expression to maintain homeostasis and cellular identity (Broders-Bondon et al., 2018; Salvi and DeMali, 2018; Kassianidou et al., 2019). Among these are the Hippo pathway proteins Yes-associated protein (YAP) and its transcriptional coactivator with PDZ-motif (TAZ), which regulate E-cadherin

junctional organization, chromatin remodeling, and even cell metabolism (Pancier et al., 2017). In fact, the Hippo pathway is known to be homologous to the septation initiation network (SIN) and mitotic exit network (MEN) in *S. pombe* and *S. cerevisiae*, respectively. These pathways coordinate chromosome segregation with cytokinesis through a sequence of signaling cascades through well-conserved kinases, their regulatory components, and scaffolding proteins (Hergovich and Hemmings, 2012; Simanis, 2015). In mammalian systems, various Hippo pathway proteins have been shown to have cell cycle progression phenotypes (Yabuta et al., 2007; Hergovich and Hemmings, 2012).

Feedback between cell mechanics and YAP is critical for cell identity determination (Dupont et al., 2011). Studies found that physiologically relevant mechanical cues, such as substrate stiffness, help dictate the differentiation of progenitor stem cells, and that myosin II plays a central role (Engler et al., 2006). Moreover, YAP translocation in and out of the nucleus in response to substrate stiffness is required for stem cells to differentiate accurately (Guilak et al., 2009; Lian et al., 2010; Smith et al., 2017; Totaro et al., 2017). This mechanically transduced transcriptional pathway also engages in positive feedback with the cytoskeletal network. YAP is not only a downstream effector of mechanical inputs, it also has a cell autonomous impact on cortical tension and works through TEAD to drive expression of key mechanical proteins, including myosin light chain (Bai et al., 2016). In addition, a recent study found that the chromatin remodeling SWI/SNF complex binds to YAP in the nucleus through ARID1A, which prevents the interaction between YAP and the transcription factor TEAD. This, in turn, prevents YAP-mediated progenitor-like properties in human mammary epithelial cells (HMECs) (Chang et al., 2018). Here, SWI/SNF functions as a negative regulator of YAP using sequestration of YAP to maintain differentiated states. Loss of ARID1A or SWI/SNF through genetic lesions may have decreased thresholds for YAP activation, leading to loss of differentiation in tumor cells (Chang et al., 2018). Similarly, the loss of negative regulation

of YAP by myosin II allows for activation of pro-growth pathways in cancer cells and tumorigenesis (Picariello et al., 2019).

YAP/TAZ also generate a negative feedback loop that is critical for maintaining persistent cell migration. YAP regulates myosin II phosphorylation through multiple compensatory pathways of myosin II light chain phosphorylation and modulates cell migration (Mason et al., 2019). Thus, while myosin II activity is critical for motility, increased activity is inhibitory to migration, highlighting the importance of both positive and negative feedback loops mediated by transcription factors to drive cellular processes. In this scenario, YAP/TAZ displays the function of both a sensor and an actuator that ultimately integrates with other feedback controllers like myosin II.

A number of recent studies have also explored the feedback between cell mechanics and metabolism. Actin dynamics affect mitochondrial fission and fusion, which in turn impacts mitochondrial function (Beck et al., 2012; Hatch et al., 2014). In addition, recruitment of mitochondria to the leading edge of a cell also promotes cell migration and invasion in tumor cells (Caino et al., 2015; Cunniff et al., 2016). Furthermore, the signaling between focal adhesions, integrins, and metabolic enzymes also provide a possible means for feedback. For example, the application of shear stress or force on E-cadherin at cell-cell junctions results in the activation and recruitment of AMP-activated protein kinase (AMPK) to adhesion complexes, which results in increased phosphorylation and activation of myosin II. This also increases glucose intake and ATP production, providing the cell with increased energy to actively respond to the change in its environment (Bays et al., 2017; Salvi and DeMali, 2018).

Moreover, AMPK signaling drives changes in cortical tension that regulates entosis, the process whereby softer cells engulf stiffer cells, that is found in many solid tumor types and likely a response to the nutrient deprivation in highly competitive growth conditions (Overholtzer et al., 2007; Sun et al., 2014; Hamann et al., 2017). In the breast

cancer cell line MCF-7, glucose deprivation results in a bimodal distribution of cells, which are characterized by either a low or high elastic modulus. The increase in elastic modulus is driven by AMPK activation, highlighting the role of AMPK as a transducer of metabolic signals to cellular mechanics (Hamann et al., 2017). More recently, another study demonstrated a myosin II-dependent increase in stiffness of brown/beige adipose tissue and isolated brown adipocytes in response to cold challenge (Tharp et al., 2018). Here, actomyosin contractility was critical for the thermogenic capacity of the cells and the induction of uncoupled respiration through YAP/TAZ-mediated gene regulation (Tharp et al., 2018). Therefore, these studies are beginning to reveal parts of the sophisticated systems that are in place to regulate cell mechanics in the context of other cellular processes.

In *Dictyostelium*, the contractility controller finely tunes the amount of contractile protein that accumulates at a site of stress through a mechanical feedback loop (Kee et al., 2012; Srivastava and Robinson, 2015). IQGAP scaffolding proteins sense inputs from small GTPases and also feedback onto the cytokinetic signaling module (Faix et al., 2001; Kee et al., 2012). Importantly, the cell has two IQGAP proteins that have opposing roles in modulating mechanoaccumulation: IQGAP1 provides an inhibitory function while IQGAP2 alleviates this inhibition (Kee et al., 2012; Srivastava and Robinson, 2015; Kothari et al., 2019b). This cross-antagonism and feedback between the signaling module, the IQGAP proteins, and the contractile machinery regulate the setpoint of this control system, which allows for a 3-5-fold dynamic range in myosin II accumulation. However, the biochemical interactions that drive this control system and the negative regulation by IQGAP1 remained unclear. In my thesis work, I have endeavored to use the model organism *Dictyostelium discoideum* to identify the biochemical interactors that builds the mechanobiome. By measuring the protein-protein interactions that drive a cell's ability to generate, sense, and respond to forces, we may begin to understand the mechanical

alterations that drive disease state progression, and ultimately develop therapeutics return these systems to their normal state.

Note: Text and figures have been adapted from (Kothari et al., 2019a).

Chapter 2 Materials and Methods

Quantitative methods that measure cell mechanics, mechanoresponse, protein dynamics, and molecular interactions are necessary to provide insight into both the mechanical and biochemical components involved in cytokinesis and cell shape regulation. Fluorescence Correlation and Cross-Correlation Spectroscopy (FCS/ FCCS) have become valuable methods for measuring protein dynamics *in vivo* that occur on nanometer to micron length-scales, and microsecond to minute time-scales. The methods provide the ability to quantify the dynamics and interactions that allow changes on the molecular level to impact the cell's ability to change shape and undergo cytokinesis. Although trans-illumination microscopy has provided us with a wealth of information regarding dividing cells, this approach fails to capture the spatial and temporal details of this complex mechanical process. While cytokinesis occurs over the time-scale of minutes, the process is driven by associations, interactions, and forces that occur on a millisecond to seconds time-scale. During any shape change process, the cell's ability to respond to various external perturbations is dependent upon transient and dynamic interactions that allow for rapid molecular-level responses. The methods described here are applicable to single-cell systems, and have been used with the social amoeba *Dictyostelium discoideum* (Kee et al., 2012; Srivastava and Robinson, 2015), *Drosophila melanogaster* S2 cells (Kim et al., 2015; Duan et al., 2018), as well as mammalian cells (Sun et al., 2014; Schiffhauer et al., 2016; Schiffhauer et al., 2019).

Reagents

The plasmids for GFP-mCherry (linked), and GFP- and/or mCherry-tagged fusions of myosin-II, myosin-II 3xAsp, cortexillin-I, IQGAP1, IQGAP2, mmsdh, Rac-1A, filamin, and RNP-1A have been described previously (Effler et al., 2006; Lee et al., 2010; Zhou et al., 2010; Kee et al., 2012; Luo et al., 2013; West-Foyle et al., 2018). For the FLAG

constructs, FLAG-GFP was cloned into the pDRH plasmid using *Bgl* II and *Sal* I restriction sites, and cortexillin I or IQGAP2 were added between *Sal* I and *Not* I restriction sites. GFP-myosin II S1-mCherry pDM181 was built by cloning the myosin II S1 fragment into GFP-pDM181 between the *Sal* I and *Not* I sites, and subsequently inserting mCherry between *Not* I and *Mlu* I sites. Discoidin-1A was cloned by PCR using template genomic DNA from the WT strain KAx3 with forward primer 5' GTCGACATGTCTACCCAAGGTTTAGTTCAACTCCTCG (including a 5' *Sal* I site), and reverse primer 5' GCGGCCGCTTATTCCAAGCGGTAGCAATGTAATCAG (including a 3' *Not* I site). The *Sal* I and *Not* I sites were then used to clone the gene into GFP-pDM181. The monoclonal antibody 241-438-1 against cortexillin I developed by Günther Gerisch (Max Planck Institute) was obtained from the Developmental Studies Hybridoma Bank (University of Iowa, Iowa City, IA). An M2 anti-FLAG antibody and anti-FLAG affinity agarose gel (F3165 and A2220, Sigma-Aldrich, St. Louis, MO) were used for IP. The myosin II heavy chain antibody (anti-my6) (Peltz et al., 1985) and anti-FLAG antibody were used for western analysis (1:10,000 and 1:1000, respectively). Biotinylated antibodies rabbit-anti-GFP (600-406-215, Rockland Immunochemicals, Pottstown, PA), rabbit-anti-RFP (ab34771, Abcam, Cambridge, United Kingdom), and rabbit-anti-HA (ab26228, Abcam) were used at 1:300 for SiMPull. Latrunculin A was obtained from Sigma-Aldrich.

Cell strains and Culture

A complete list of the strains used is provided in **Table 1**. Cells were grown in Hans' enriched 1.5x HL-5 media, enriched with 8% FM, containing penicillin and streptomycin, at 22°C on polystyrene petri dishes. Wild-type strains used were KAx3 and rescued strains (Ruppel et al., 1994). Mutant cell lines used have been previously described: *myoII*, *cortI*, *cortI/II*, *iqg1*, *iqg2*, and *iqg1/2* (Robinson and Spudich, 2000; Lee et al., 2010). Cells were transformed with the expression plasmids by electroporation using

a Genepulser-II electroporator (Bio-Rad, Hercules, CA). Cells were then grown in selection with media containing 15 $\mu\text{g}/\text{mL}$ G418, 40 $\mu\text{g}/\text{mL}$ hygromycin, or both drugs when transforming two plasmids. Expression levels were checked by fluorescence imaging or Western analysis. For Latrunculin A treatment, cells were pre-treated with 0.1% DMSO for 4 hrs. Cells plated in imaging chambers were washed with low flow media with 0.1% DMSO, and were incubated with 5 μM Latrunculin A diluted in low flow media for 10 min. Slides were changed after 15 min of imaging.

Table 1. List of Dictyostelium strains used.

Background Strain	Plasmids transformed
<i>myoII</i>	mCherry-myosin II pDRH; 14-3-3 GFP pLD1
<i>myoII</i>	GFP-myosin II pDRH; mCherry-YHWAQ pDM181
<i>myoII</i>	GFP-myosin II pDRH; mCherry-YHWAS pDM181
<i>cortI</i>	FLAG-GFP-cortexillin I pDRH; pDM181
<i>cortI</i>	FLAG-GFP pDRH; pDM181
<i>iqg2</i>	FLAG-GFP-IQGAP2 pDRH; pDM181
<i>iqg2</i>	FLAG-GFP pDRH; pDM181
<i>cortI/II</i>	FLAG-GFP-IQGAP2 pDRH; pDM181
<i>cortI/II</i>	FLAG-GFP pDRH; pDM181
KAx3	FLAG-GFP pDRH; pDM181
KAx3	GFP pDM181; mCherry pDRH
KAx3	GFP-5aa-mCherry pDM181; pDRH
<i>myoII</i>	GFP-myosin-II pBig; mCherry pDRH
<i>myoII</i>	GFP-myosin S1-mCherry pDM181
<i>myoII</i>	GFP-myosin-II pBig; mCherry-cortI pDRH
<i>myoII</i>	GFP-IQGAP2 pExp4; mCherry-myosin-II pDRH
<i>myoII</i>	GFP-myosin II pBig; mCherry-IQGAP2 pDRH
<i>myoII</i>	GFP-myosin II-3xAsp pBig; mCherry-IQGAP2 pDRH
<i>myoII</i>	GFP-IQGAP2 pExp4; mCherry-cortI pDRH
<i>cortI</i>	GFP-IQGAP2 pExp4; mCherry-cortI pDRH
<i>cortI</i>	GFP-myosin-II pBig; mCherry-cortI pDRH
<i>cortI</i>	GFP-IQGAP2 pExp4; mCherry-myosin-II pDRH
<i>iqg1</i>	GFP-myosin-II pBig; mCherry-cortI pDRH
<i>iqg1</i>	GFP-IQGAP1 pExp4; mCherry-cortI pDRH
<i>iqg1</i>	GFP-myosin-II pBig; mCherry-IQGAP1 pDRH
<i>iqg1</i>	GFP-IQGAP2 pExp4; mCherry-myosin-II pDRH
<i>iqg2</i>	GFP-myosin-II pBig; mCherry-cortI pDRH
<i>iqg2</i>	GFP-IQGAP2 pExp4; mCherry-cortI pDRH
<i>iqg2</i>	GFP-IQGAP2 pExp4; mCherry-myosin-II pDRH
<i>iqg2</i>	GFP-myosin II pBig; mCherry-IQGAP2 pDRH
<i>iqg1/2</i>	GFP-IQGAP2 pExp4; mCherry-cortI pDRH
<i>iqg1/2</i>	GFP-IQGAP2 pExp4; mCherry-myoII pDRH
<i>iqg1/2</i>	GFP-myosin-II pBig; mCherry-cortI pDRH
KAx3	14-3-3-GFP pLD1; pREP
<i>cortI</i>	GFP-mmsdh pDM181; mCherry-cortI pDRH
<i>myoII</i>	GFP-mmsdh pDM181; mCherry-myoII pDRH
<i>cortI</i>	GFP-Rac1A pDM181; mCherry-cortI pDRH
<i>cortI</i>	GFP-RNP-1A pLD1; mCherry-cortI pDRH
<i>cortI</i>	GFP-Filamin pDXA; mCherry-cortI pDRH
<i>cortI</i>	GFP-Discoidin 1A pDM181; mCherry-cortI pDRH
<i>iqg2</i>	GFP-Rac1A pDM181; mCherry-IQGAP2 pDRH
<i>iqg1</i>	GFP-Rac1A pDM181; mCherry-IQGAP2 pDRH
<i>cortI</i>	GFP-Rac1A pDM181; mCherry-IQGAP2 pDRH
<i>iqg2</i>	GFP-Filamin pDXA; mCherry-IQGAP2 pDRH
<i>iqg1</i>	GFP-Filamin pDXA; mCherry-IQGAP2 pDRH
<i>iqg2</i>	GFP-Discoidin 1A pDM181; mCherry-IQGAP2 pDRH
<i>orfJ</i>	GFP-myosin II 3xAsp; pLD1
<i>orfJ</i>	GFP-myosin II 3xAsp; mmsdh pLD1

Anti-FLAG Co-immunoprecipitation

Logarithmically growing cells (*cortl*::FLAG-GFP-*cortl*, *cortl*::FLAG-GFP, *iqg2*::FLAG-GFP-IQGAP2, *iqg2*::FLAG-GFP; *cortl*//*ll*::FLAG-GFP-IQGAP2; *cortl*//*ll*::FLAG-GFP) were collected, washed in 1X phosphate buffered saline, and resuspended in lysis buffer (100 mM PIPES pH 6.8, 2.5 mM EGTA, 1 mM MgCl₂, 1 mM ATP, 0.1% Triton X-100, and protease inhibitor cocktail) at a cell density of 1 x 10⁷ cells/mL. Cells were incubated with rotation at 4°C for 30 min and lysates were centrifuged at 15,000 x g for 5 min at 4°C to separate the soluble and cytoskeletal fractions. The pellet from the 'cytoskeletal' sample was dissolved in Release Buffer (100 mM PIPES pH 6.8, 2.5 mM EGTA, 1 mM MgCl₂, 1 mM ATP, 200 mM NaCl and protease inhibitor cocktail), and incubated on a rotator for 15 min at 4°C. The 'cytoskeletal' sample was then centrifuged at 15,000 x g for 5 min at 4°C, and the supernatant was processed for co-immunoprecipitation. Lysates were pre-cleared with agarose-bead-conjugated mouse IgG (Sigma-Aldrich) for 30 min and centrifuged at 5000 x g for 1 min. Supernatants were transferred to tubes containing 40 µL pre-washed agarose-bead-conjugated-anti-FLAG antibody (Sigma-Aldrich) overnight at 4°C. The resin was washed four times with 1X TBS, and eluted with sample buffer for western analysis.

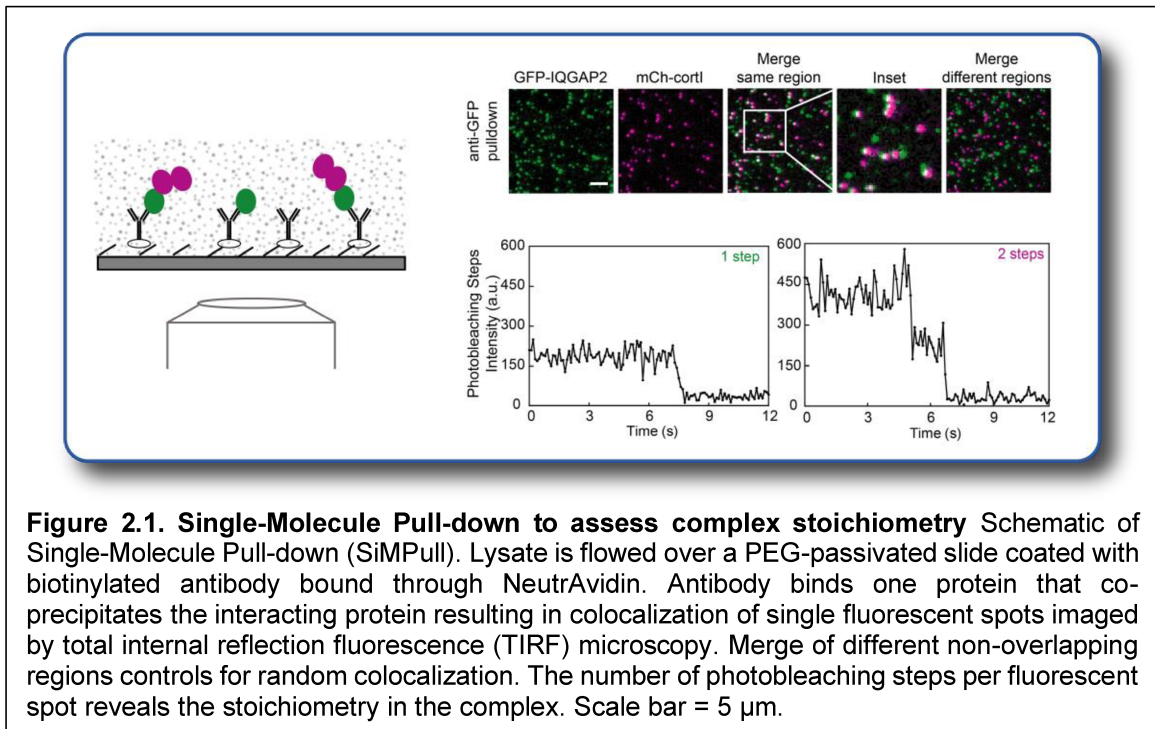
Single-Molecule Pull-down (SiMPull)

We can use single-molecule pull-down to measure the stoichiometries of proteins in complexes. Proteins of interest fused with fluorescent proteins are co-expressed in cells. Transformed cells were washed once in 1X phosphate buffered saline, resuspended in lysis buffer (as described above) at a cell density of 5x10⁷ cells/mL. Cells were rotated at 4°C for 15 min, and centrifuged at 15,000 x g for 5 min to remove cell debris. Lysate was added to slides coated with biotinylated antibodies as previously described

(Husbands et al., 2016). Biotinylated antibodies immobilized in flow chambers using NeutrAvidin (Thermo Fisher Scientific) were used to pull-down one protein of interest, and single-molecule TIRF imaging with a 100x objective was used to image both GFP and mCherry-labeled proteins (**Fig. 2.1**). Areas with approximately 200-800 molecules were imaged to avoid overlapping fluorescence signal due to spatial proximity. Colocalization was quantified using **Equation 1** for each antibody (where X is the protein pulled down).

$$\text{colocalization with antibody against X} = \frac{\text{number of colocalized spots}}{\text{number of X spots}}. \quad (1)$$

Photobleaching analysis was performed as described (Husbands et al., 2016). Anti-HA was used as a control antibody to demonstrate low level of non-specific pull-down of fluorescently labeled proteins.



Fluorescence Correlation Spectroscopy (FCS)

The diffusion and mobility of a protein dictates its lifetime dynamics and the complexes it may be part of. This information is invaluable for developing quantitative models that explain the behavior of the individual protein, and ultimately, the process in which it participates. Macromolecules can passively diffuse or actively move within the cytoplasm of a cell. Passive diffusion is dependent upon the viscosity of the cytoplasm and the size and shape of the molecule, occurring on the order of $5 \mu\text{m}^2/\text{s}$. Molecular motors, such as kinesin and myosin, drive directed transport along microtubules and actin, moving cargo on the order of $1 \mu\text{m}/\text{s}$. Molecular motors can also “stir” the cytoplasm, actively increasing the apparent diffusion of a protein (Guo et al., 2014). Determining diffusion times of proteins may help decipher mechanisms of a process, and help establish mathematical models that predict biological behavior. Models that describe the mechanosensing behavior of proteins and the cortical viscoelasticity of the cell enhance our understanding of the role of a mechanical meshwork of actin, motors, and crosslinking proteins during furrow ingression (Luo et al., 2012; Poirier et al., 2012; Luo et al., 2013; Mohan et al., 2015).

Fluorescence Correlation Spectroscopy (FCS) is a particularly powerful method for measuring diffusion and mobility inside cells. FCS has been used to measure diffusion of molecules *in vitro* and *in vivo*, under different stages of the cell cycle and mechanical and pharmacological perturbations. Diffusion and mobility parameters can be extracted from the intensity fluctuations of a fluorescently-labeled protein or molecule in a confocal voxel. A correlation function is used to determine the number of fluorescent particles present in the volume over the time course, and single- or multiple-component fits are used to calculate the diffusion time, which is the average time required to diffuse across the confocal volume. The diffusion time extracted is then used to determine diffusion coefficients. This quantitative analysis also provides information on complex assembly and

concentration changes. A change in a protein's diffusion time can reflect a change in the cytoskeletal and biochemical interactions in the network. For example, changes in the dynamics of cortexillin I, an actin-bundling protein, and IQGAP2, a scaffolding protein, were studied by FCS in different genetic backgrounds of *Dictyostelium* cells. In an *iqgap2* null background, cortexillin I showed a 30% increase in cytoplasmic diffusion time, suggesting that it engages in different biochemical interactions when IQGAP2 is absent (Srivastava and Robinson, 2015). In addition, FCS was used to demonstrate that global mechanical stresses change protein dynamics, as cortexillin I in compressed cells had two-fold slower diffusion rates (Srivastava and Robinson, 2015). The ability to study these dynamics in live cells on the microsecond and nanometer scale is crucial for understanding how changes in the cell cycle and external perturbations affect protein diffusion and mobility, which ultimately affect the cell's biochemistry.

Experimental Setup

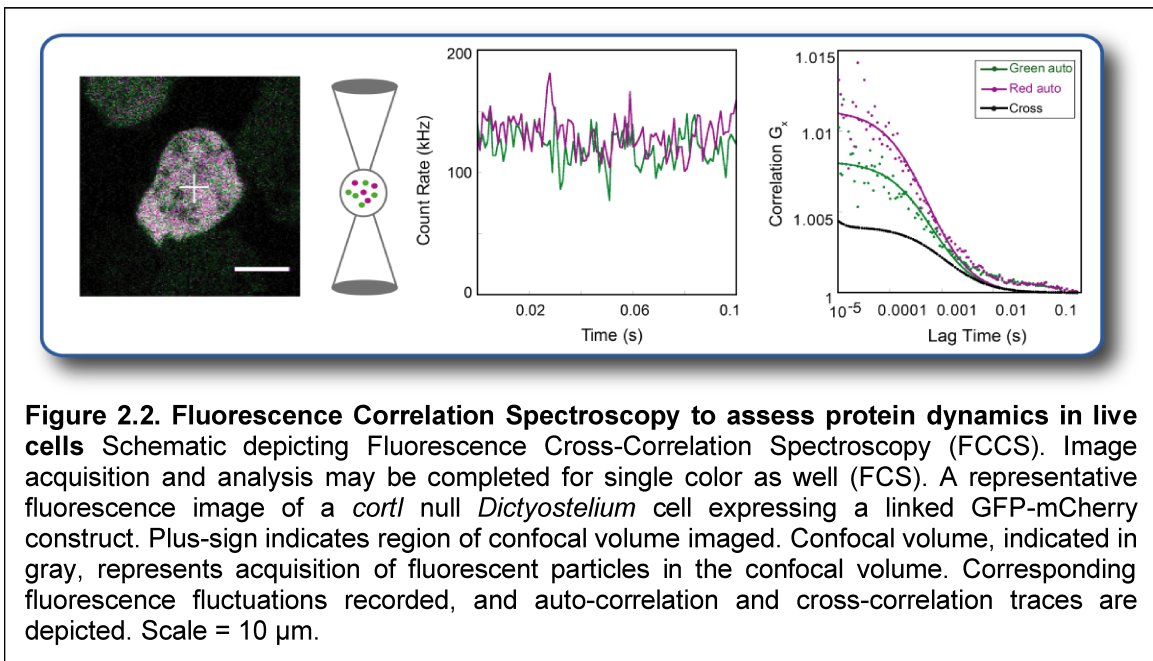
FCS experiments were performed on interphase cells as described at ambient temperature (~20-23°C, normal growth temperatures for *Dictyostelium* cells) using a Zeiss AxioObserver with 780-Quasar confocal module & FCS, with a C-Apochromat 40x (NA 1.2) water objective to image a confocal volume of approximately 0.5 femtoliter (Srivastava and Robinson, 2015; West-Foyle et al., 2018) An avalanche photodiode detects the fluorescence fluctuations within the volume and the signal is auto-correlated over time (**Fig. 2.2**) (Bacia et al., 2006; Bulseco and Wolf, 2013). Having a small number of particles, ideally less than 100, in the volume is essential for accurately identifying small changes. Software, such as Zen, include equations with single- or multiple- component fits to determine correlation values and diffusion times (Carl Zeiss Microimaging, Guide to Basic FCS Experiments). Fluorescence fluctuations are the result of species mobility, as well as various inter- and intramolecular interactions. Fluctuations may also occur due to a change

in intrinsic fluorescence, often from a triplet state, in which the fluorophore has transitioned to a dark state. To correct for this, a triplet-state component must be added to the model.

Correlating the fluorescence fluctuations over time yields a plot as seen in **Figure 2.2**. After accounting for the triplet state, the peak correlation amplitude is the auto-correlation value (G_x). The algorithm extracts the particle number ($G_x = 1/N$, where N is the number of particles); a smaller particle number will have a greater auto-correlation value. The diffusion time is extracted from the decay of the slope, and a diffusion coefficient may be calculated by **Equation 2**, the Stokes-Einstein equation:

$$D = \frac{k_B T}{6\pi\eta r}, \quad (2)$$

where k_B is the Boltzmann constant, T is temperature, η is the viscosity, and r is the Stokes radius of the particle.



I. Calibration of the system

Calibrating the system using a fluorescent molecule with a known diffusion coefficient allows for measurement of the size and shape of the confocal volume created by the laser

and pinhole. 100 nM Rhodamine 6G was used for pinhole alignment and structural parameter calculation as previously described (Srivastava and Robinson, 2015). A structural parameter of 6 was used and the confocal volume was measured to be 0.45 fL (Bacia et al, 2006; Srivastava and Robinson, 2015). The correction collar of the objective must be adjusted to achieve the highest count rate from the dye. This adjustment corrects for the thickness of the cover glass. Next, the pinhole must be aligned; most software packages have automatic adjustments in the x and y directions to maximize the count rate from the dye. The pinhole should be set to one airy unit to create the smallest confocal volume possible.

II. Monitoring fluorescence fluctuations

When imaging the calibration dye or a fluorescently-labeled species in solution, images can be acquired continuously for ten seconds with ten repetitions. When imaging in live cells, shorter acquisition times with fewer repetitions (we typically use five repetitions of two-second time-lapses for *Dictyostelium*) should be used to avoid artifacts from active cell migration and photobleaching. While *Dictyostelium* were imaged at ambient room temperature (approximately 25°C), mammalian cells were allowed to settle on glass coverslips overnight and imaged at 37°C and 5% CO₂.

III. Fitting to models

The fluorescence fluctuations over time are analyzed to yield an auto-correlation value, G_x (**Equation 3**):

$$G_x = \frac{\langle \delta F(t) \cdot \delta F(t + \tau) \rangle}{\langle F(t) \rangle^2}, \quad (3)$$

where t is time and $F(t)$ is the fluorescence fluctuation detected. While G_x is a value from 0 to 1, 0 being no correlation and 1 being complete correlation, the software adjusts this range from 1 to 2 to simplify calculations (Bulsecu and Wolf, 2013).

The structural parameter is the ratio of the axial resolution to the radial resolution and is typically between 5 and 7. This is calculated from the diffusion time of the calibration dye. To account for the triplet state excitation, a triplet state component is added to the fit. However, since this state should be rapid, its fit should be restricted to a maximum of 8 μ s. Thus, data was fit to a single-component 3D diffusion model, including a triplet-state component with an upper limit of 8 μ s (as described in (Kothari et al., 2017)). In addition, the data can be fit to a single-component or multiple-component 3D diffusion model, depending on the species measured. Because the algorithm may not correctly identify separate groups within the data, we focused on simpler models that include single components. The data are then fit to a one-component model to generate a parameter set that may represent a distribution of species.

IV. Data analysis

Once the correlation plots have been fit to the models, the resulting parameters can be analyzed to extract information on the number of species within the volume and their average diffusion time. However, not every trace may fit the model well. The residual trace shows how the data deviates from the fit and is helpful in determining whether the model is an accurate representation of the data. Occasionally, the fluorescently-labeled species may aggregate, either in solution or in live cells. During live cell FCS, an organelle or large fluorescing species may enter the imaging volume. Such aggregates or disturbances can be detected in the trace as significant deviations or non-uniform fluctuations in the count rate. These traces may be removed from the analysis. Traces that show photobleaching

over time should also be discarded. The remaining traces are averaged, the data is fit to the model, and an average diffusion time is extracted. This diffusion time can then be converted into a diffusion coefficient using the dye as calibration for the confocal volume shape and size. This analysis is used to measure diffusion times, and also to determine the assembly of complexes, binding stoichiometry, and changes in the network. To measure interactions between two specific proteins or molecules, FCS may be performed with two colors, a technique known as Fluorescence Cross-Correlation Spectroscopy (see next).

Fluorescence Cross-Correlation Spectroscopy (FCCS)

Fluorescence Cross-Correlation Spectroscopy (FCCS) involves imaging intensity fluctuations of two different fluorophores within the same focal volume. A significant cross-correlation between the species suggests that the two species might associate based on the probability of the two different fluorophores diffusing in or out of the volume simultaneously. FCCS allows for quantitative interaction measurements between two species *in vitro* and detection of associative interactions *in vivo*, yielding information on interaction strengths, dissociation constants, and binding stoichiometries. Traditional methods of studying protein-protein interactions in cells, such as co-immunoprecipitation (co-IP) and Förster Resonance Energy Transfer (FRET), have their own significant limitations. Co-IP requires lysing the cells and a time delay as the extracts are exposed to beads, washed, and eluted; this readily detects very stable associations, but disrupts more transient ones. FRET requires that the donor and acceptor fluorophores reside within a minimal distance in a relatively optimal orientation. FCCS circumvents both types of issues; cells remain intact, and fluorophores do not have to reside within an optimal distance or orientation. Performing FCCS *in vivo* facilitates analysis of protein-protein interactions in context and allows for the relatively easy process of incorporating acute

and genetic perturbations. In the context of cytokinesis, it allows for a comparison between interactions at the cleavage furrow and those that occur globally. In addition, FCCS is sensitive enough to identify transient interactions that may not be detectable by co-IP (Bacia et al., 2006; Bacia and Schwille, 2007).

FCCS requires that two species be labeled with different fluorophores with little overlap in excitation and emission spectra to prevent cross-talk. However, the confocal volumes must have significant overlap to allow for accurate cross-correlation. If the system has one confocal pinhole, then the volume must be adjusted to a single wavelength. However, if two pinholes are used, the two volumes may be set for closer overlap. Although FCCS *in vitro* can provide reliable measurement of a dissociation constant, K_d , measurement *in vivo* is limited to relative interaction strengths. This limitation comes from the fact that proteins may be involved in interactions with multiple cellular factors, which complicates the measurement of a true K_d . Further, expression of the fluorescent protein in addition to an unlabeled endogenous population complicates the K_d assessment as well. In addition, the presence of organelles and cytoskeletal networks will also affect cross-correlation. However, the relative interaction strength is still a valuable measurement for characterizing novel, transient interactions that have an impact on biological processes.

For negative controls, we measured the interaction between co-expressed soluble GFP and mCherry, as well as co-expressed soluble mCherry and GFP-myosin, to compensate for the slower diffusion time of larger proteins. As positive controls, we compared the interaction between GFP attached to mCherry by a 5-amino acid flexible linker as well as fluorophores linked by the myosin II S1 fragment. Where possible, we also switched fluorophores to ensure binding affinities were not dependent upon fluorophore interactions. In addition, to confirm the full range of the experimental setup, we measured dual-color fluorescent beads in solution, which showed maximal auto- and cross-correlations of 0.25 and a measured K_D of 1 pM.

The *in vivo* K_D was calculated using **Equation 4**, where N is Avogadro's number, V is volume, G_x is the cross-correlation and G_a and G_b refer to the auto-correlation values for GFP and mCherry as extracted from the Zen imaging software (Bierbaum and Bastiaens, 2013; Kothari et al., 2017; West-Foyle et al., 2018).

$$in\ vivo\ K_D = \frac{G_x}{N \cdot V \cdot G_a \cdot G_b} \cdot \left(\frac{G_a}{G_x} - 1\right) \cdot \left(\frac{G_b}{G_x} - 1\right). \quad (4)$$

The cross-correlation function, G_x , is a measure of how well the fluorescence fluctuations from the two different channels correlate over time, and is calculated using **Equation 5**:

$$G_x = \frac{\langle \delta F_A(t) \cdot \delta F_B(t + \tau) \rangle}{\langle F_A(t) \rangle \langle F_B(t) \rangle}, \quad (5)$$

where t is time, and $F(t)$ is the fluorescence fluctuation in either the green or red channel. The cross-correlation value ranges from 0 to 1, with 0 being no cross-correlation, and 1 being complete correlation. The scale is again adjusted from 1 to 2, and we find that values generally range between 1.001 to 1.1 in live cells, and between 1.05 to 1.2 for species in solution.

The experimental setup used for FCCS is similar to the one used for FCS, but the additional laser that excites the second fluorophore creates a second confocal volume. When acquiring traces, the two lasers simultaneously excite the sample, and fluorescence fluctuations from both channels are recorded. This results in three plots: two auto-correlation plots (one for each channel), and one cross-correlation plot. The traces with aggregates or photobleaching are discarded, and the correlations are fit to the model.

Fluorescence Recovery after Photobleaching (FRAP)

Fluorescence Recovery after Photobleaching (FRAP) is a commonly used technique to measure turnover dynamics of proteins in cells. A region of a cell expressing the fluorescent protein of interest is photobleached using a laser, and that region is imaged over time to measure the rate of fluorescence recovery by unbleached, fluorescent molecules from outside the region (Jacobson et al., 1976; Lippincott-Schwartz et al., 2001). The resulting recovery curve can be used to calculate the rate of movement, the release time from other binding interactions, and the fraction of the protein that is mobile. For proteins that recover on the order of hundreds of milliseconds to seconds, the recovery time is generally dominated by the unbinding kinetics of the protein from its binding partners. This unbinding may reflect the release time of the bleached protein or, more commonly, release of the unbleached protein from nearby pools. In contrast, a protein with low turnover dynamics may be incredibly stable. Proteins may also fail to recover to the initial fluorescence intensity due to their deep associations in larger complexes and networks. Once the images have been corrected for photobleaching, the percent recovery represents the population of the protein that is mobile within the cell.

Experimental Setup

A few images of the region of interest are taken to quantify the intensity of the fluorescence before photobleaching. A small region is photobleached with a laser of the excitation wavelength of the fluorescent protein. This region is then imaged over time until recovery has saturated. An unbleached region of the cell is also imaged simultaneously to account for photobleaching due to image acquisition over time. The average intensity of the bleached region, the control unbleached region, and background are quantified.

After background correction, the intensity is fit to a single exponential form, **Equation 5**:

$$NI(t) = m_1(1 - m_2 \cdot e^{-kt}), \quad (5)$$

where m_1 and m_2 are fitting parameters. The immobile fraction may be quantified by

Equation 6:

$$F_i = \frac{1 - m_1}{1 - m_1 + m_2}, \quad (6)$$

Quantifying this recovery of intensity can yield insight into the kinetics and complexes of protein dynamics (Srivastava and Robinson, 2015).

Agarose Overlay

Agarose overlay is used to apply a global compressive stress to cells (Kee et al., 2012). Proteins that are mechanoresponsive respond by accumulating at the cell cortex. Thin sheets of 2% agarose in MES starvation buffer (50 mM MES pH 6.8, 2 mM MgCl₂, and 0.2 mM CaCl₂) were made as described previously (Kee et al., 2012; Srivastava and Robinson, 2015). Cells were plated for one hour before changing the media to MES starvation buffer and imaging the cells in their normal, uncompressed state. A sheet of agarose was placed on the cells and the buffer below was removed. Imaging was started after cells appeared flattened (~2-5 minutes). Cells were imaged for 10 minutes before changing slides.

Statistics

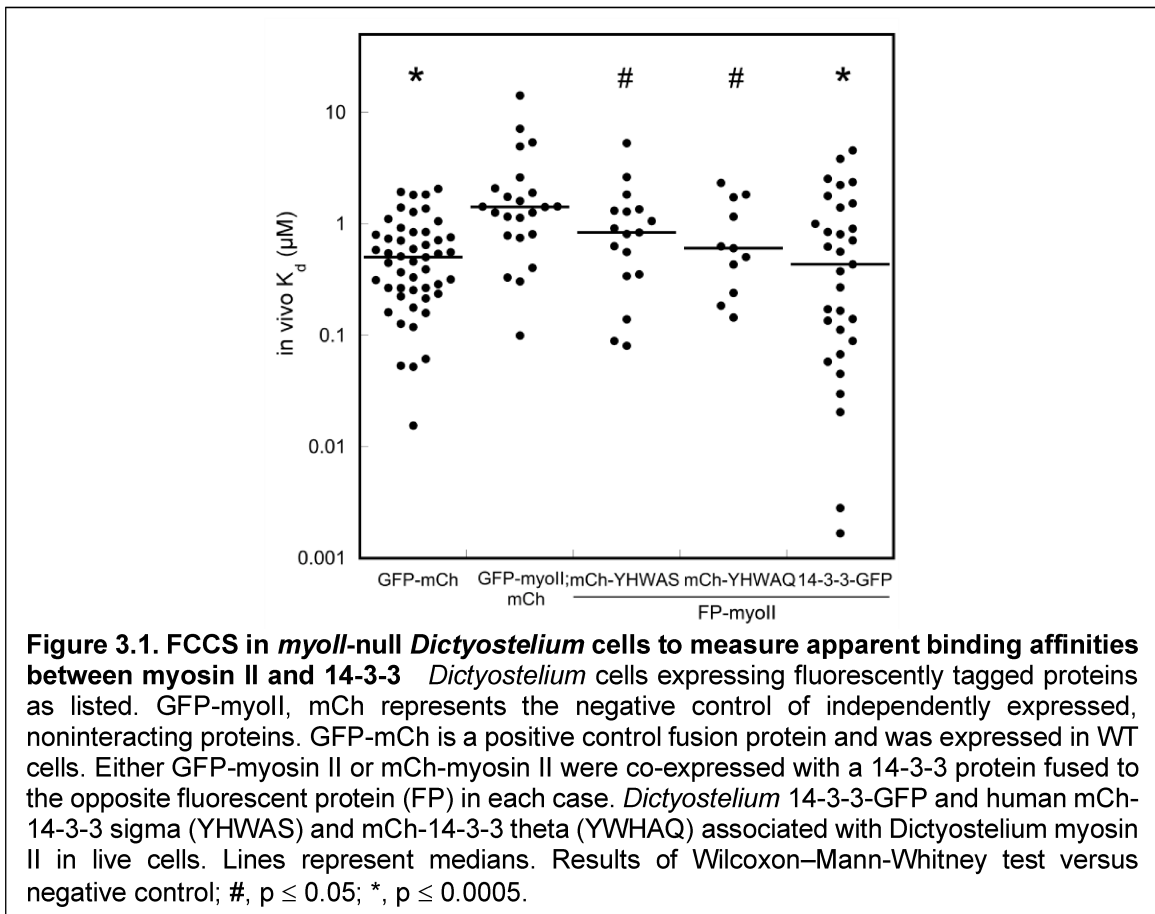
Pre-established data inclusion/ exclusion criteria: For FCCS, a single cell trace was only excluded if photobleaching was detected or the count rate deviated over 50%, indicating the presence of an organelle or aggregate diffusing through the confocal volume. For SiMPull, images were only excluded from analysis if molecules were pre-bleached due to an acquisition issue during the experiment.

Statistical analysis: An ANOVA followed by a Fisher's Least Square Difference post hoc test ($\alpha < 0.05$) or Kruskal-Wallis followed by a Wilcoxon-Mann-Whitney test was used. Statistical analysis was performed using KaleidaGraph (Synergy Software) or the Hartigans' dip test for unimodality (R statistical package).

Note: Text and figures from this section have been adapted from (Kothari et al., 2017; Kothari et al., 2019b).

Chapter 3 Using FCCS to measure *in vivo* binding affinities

As described above, FCS and FCCS are valuable tools to measure biophysical parameters within a living cell. An interaction between myosin II and scaffolding protein 14-3-3 was initially discovered through a genetic suppression selection of nocodazole in *Dictyostelium* (Zhou et al., 2010). Further *in vitro* biochemical studies with purified protein identified 14-3-3 as a direct binder and inhibitor of myosin II tail fragment assembly (West-Foyle et al., 2018). However, whether this 14-3-3 and myosin II interaction occurred in cells was unclear. Therefore, we used FCCS to measure the *in vivo* K_D between myosin II and 14-3-3 in *Dictyostelium* cells. With FCCS, we monitored the correlation between intensity fluctuations of two fluorescently-labeled proteins expressed in cells over time. We co-expressed mCherry-myosin II and 14-3-3-GFP in a *myoII* null background, thus



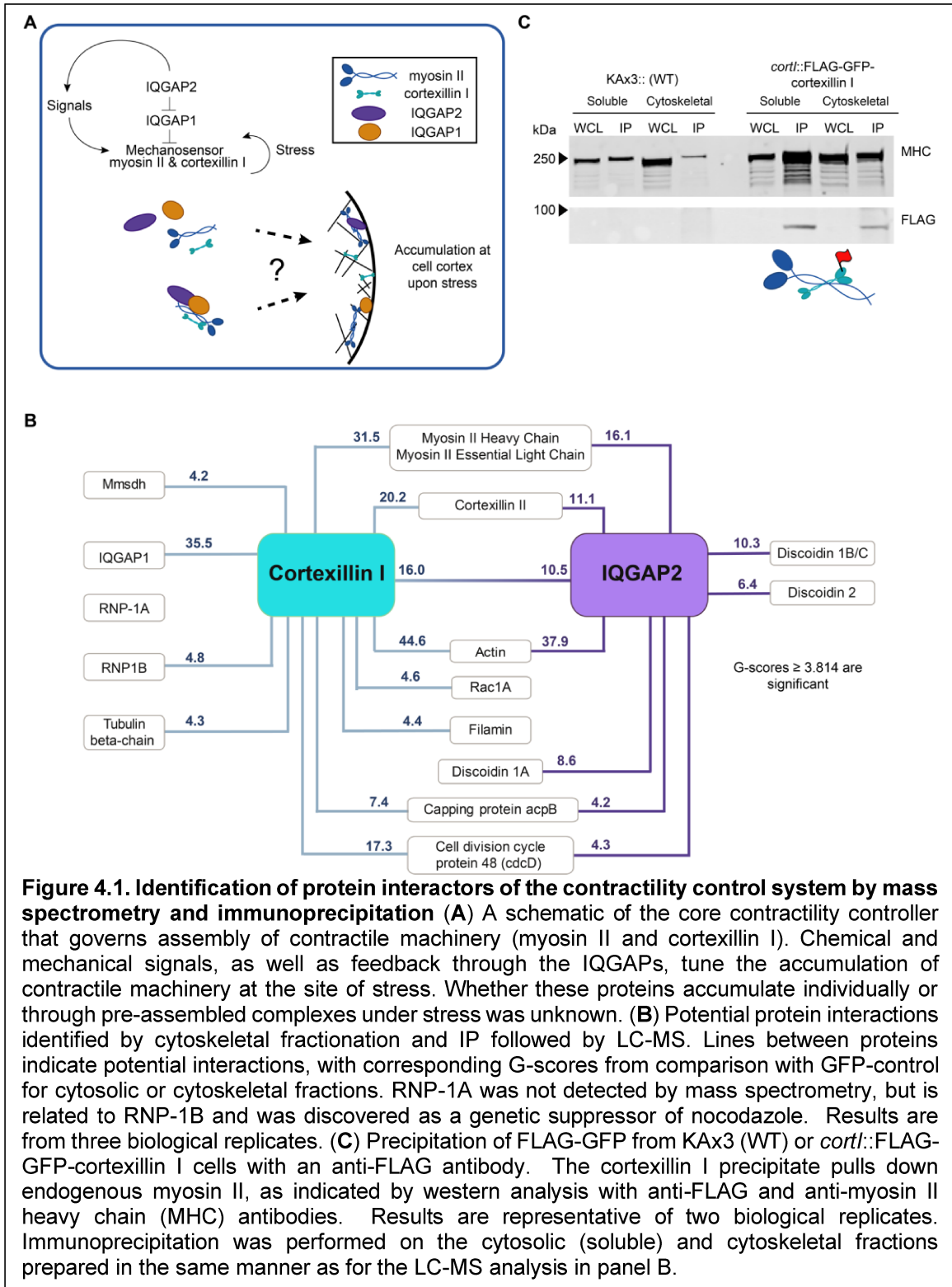
eliminating any endogenous myosin II. However, because 14-3-3 is an essential protein, its gene cannot be deleted. In comparison to the GFP-mCherry fusion positive control, which measured an *in vivo* K_D of $0.62 \pm 0.075 \mu\text{M}$, the negative control (cells co-expressing GFP-myosin II and mCherry alone) measured $1.43 \pm 0.63 \mu\text{M}$. We then measured the association between mCherry-myosin II and 14-3-3-GFP to be $0.90 \pm 0.21 \mu\text{M}$, which was significantly different from the negative control, suggesting that indeed myosin II and 14-3-3 interact in the same complex in live cells (**Fig. 3.1**). Interestingly, titration experiments of purified myosin II tail fragment against 14-3-3 measured an apparent K_D of $0.45 \pm 0.25 \mu\text{M}$, which is within range of the measured value from FCCS, suggesting that at least in this case, the *in vivo* K_D values measured are comparable to those measured *in vitro*.

In addition to studying these interactions with *Dictyostelium* proteins, purified mammalian 14-3-3 isoforms, including σ and θ , also solubilized myosin IIA (human), myosin IIB (human), and myosin IIC (mouse) tail fragments. Because of the high sequence identity between 14-3-3s from *Dictyostelium* and humans, we explored the interactions between *Dictyostelium* myosin II and human 14-3-3 proteins. Indeed, in *Dictyostelium*, human mCherry-labeled 14-3-3s σ and θ also interact with GFP-myosin II by FCCS, returning *in vivo* K_D values of $1.2 \pm 0.31 \mu\text{M}$ and $0.89 \pm 0.23 \mu\text{M}$, respectively (**Fig. 3.1**). This work, in combination with the *in vitro* biochemistry, genetics, and biophysical measurements, supports the hypothesis that 14-3-3 directly binds myosin II inhibits assembly into bipolar thick filaments. This regulation provides insight into a mechanistic link between microtubule dynamics, small GTPase RacE, and myosin II assembly that controls cortical dynamics and cell shape change (Zhou et al., 2010).

Note: Text and figures from this section have been adapted from (West-Foyle et al., 2018).

Chapter 4 Contractility kits promote assembly of the mechanoresponsive cytoskeletal network

As mentioned before, the molecular mechanisms and biochemical interactions through which mechanoresponsive proteins accumulate at the sites of stress in the cortex are poorly understood. One possibility is that diffusion-dependent encounters with the cortex allows for proteins to bind the cytoskeletal network individually, eventually leading to accumulation. Alternatively, pre-assembled complexes, or “assembly kits”, of mechanoresponsive proteins may exist in the cytoplasm, ready to engage with the cortical network upon the detection of two events: (1) encountering the cortex upon diffusion and (2) sensing a specific chemical or mechanical signal. These assembly kits may then be unpacked, providing all the necessary components for mechanoresponse, thus permitting a faster response to mechanical stress than if the proteins had to accumulate individually (**Fig. 4.1A**). However, such a view of mechanoresponse has not been explored.



Identification of direct, biochemical interactions within the mechanobiome

We first identified the molecular interactions that might be central to the mechanobiome using a proteomics approach in *Dictyostelium*. We used immunoprecipitation followed by liquid chromatography-mass spectrometry (LC-MS) to detect biochemical interactors of two key nodes, IQGAP2 and cortexillin I. We used cytoskeletal fractionation to identify protein interactions in the cytoplasm and in the cortical cytoskeleton. By doing so, we aimed to increase the likelihood of identifying key interactors, which could differ between these cellular compartments. Performing LC-MS on cytosolic and cytoskeletal precipitates of FLAG-GFP-IQGAP2 in an *iqg2* null and FLAG-GFP-cortexillin I in a *cortI* null allowed us to identify relevant molecular complexes, as well as novel regulators of contractility. As cortexillins are major interactors of the IQGAPs (Faix et al., 2001), we also carried out proteomic analysis on IQGAP2-binding proteins in a *cortIII* null background to identify cortexillin-independent interactions. G-score analysis identified 51 and 24 unique binding partners of cortexillin I and IQGAP2, respectively. Consistent with previous reports, we confirmed the IQGAP2-cortexillin I interaction, as well as cortexillin I interactions with Rac1A, IQGAP1, and cortexillin II, thereby validating our approach (Faix et al., 1998; Faix et al., 2001; Lee et al., 2010; Mondal et al., 2010). Interestingly, IQGAP1 did not co-precipitate with IQGAP2, suggesting two separate cellular pools of cortexillin I-IQGAP complexes.

We compared the significant hits with other proteins we have previously implicated in the mechanobiome, generating a list of fourteen potential interactors of cortexillin I and IQGAP2 (**Fig. 4.1B**). Interestingly, several hits were previously discovered through genetic suppression selections in *Dictyostelium*. We detected methylmalonate-semialdehyde dehydrogenase (*mmsdh*), an enzyme that catalyzes the production of propionyl- and acetyl-coA, as an interactor of cortexillin I. Overexpression of *mmsdh* was previously shown to suppress the dominant-negative phenotype of a myosin II

phosphomimetic in *Dictyostelium* (Ren et al., 2014). RNA-binding protein 1B (RNP-1B) was also identified as a binding partner of cortexillin I, which is curious since overexpression of the related protein RNP-1A suppresses the effect of nocodazole on growth of *Dictyostelium* (Zhou et al., 2010; Ngo et al., 2016). The galactose-binding lectin discoidins, which were previously demonstrated to be genetic suppressors of *cortI* null cells (Robinson and Spudich, 2000), were detected as interactors with IQGAP2 by proteomics in the presence of cortexillin I and II.

In addition, several cytoskeletal proteins emerged as cortexillin I and IQGAP2 binding partners and were detected in the absence of actin, suggesting they directly interact or exist in complexes within the cytoplasm independent of actin filaments. Actin precipitated in the cytosolic fraction of cortexillin I, which is expected since cortexillin I is known to bind and cross-link filamentous actin. However, actin was undetectable in the cytoskeletal fraction of the cortexillin I precipitate, which was isolated by salt extracting the initial pellet isolated during preparation of the cytosolic fraction. In this cortexillin I cytoskeletal fraction, we still detected interactions with myosin II, cortexillin II, IQGAP1, IQGAP2, Rac1A, and RNP-1B, indicating that these are not simply indirect interactions through the actin cytoskeletal network. In addition, actin was absent from the soluble precipitate of IQGAP2 in the complemented *iqg2* null and *cortI/II* null background, where interactions with myosin II, capping protein *acpB*, and cell division cycle protein 48 were still detected.

Significantly, myosin II (heavy chain and the essential light chain) emerged as a strong interactor of cortexillin I and IQGAP2 in the cytoskeletal and cytosolic fractions (**Fig. 4.1B**), suggesting that large multi-protein complexes exist within the cell cortex and cytoplasm. The IQGAP2-myosin II interaction was preserved in the *cortI/II* background, indicating that this association occurs independently of cortexillin. The saturating Mg^{2+} -ATP conditions during the immunoprecipitations, which minimize stable myosin II-

actin binding, and the absence of actin in the cortexillin I cytoskeletal fraction and IQGAP2 cytosolic fraction precipitates indicate that actin is not necessary for these interactions. We also validated the cortexillin I-myosin II association through co-immunoprecipitation with FLAG-GFP-cortexillin I in the cytosolic and cytoskeletal fractions (**Fig. 4.1C**). Given the importance of cortexillin I, IQGAP2, and myosin II in the contractility controller, we next characterized these interactions *in vivo*, studying their associations in the relevant context, rather than in cell lysates.

Cortexillin I and IQGAP2 interact with myosin II *in vivo*

We used Fluorescence Cross-Correlation Spectroscopy (FCCS) in live interphase cells to quantitatively characterize key protein interactions identified through mass spectrometry within their native cytoplasmic environment. Interactions were measured in each corresponding complemented-null background wherever possible to account for unlabeled protein in the cell.

We again measured *in vivo* K_D values of positive and negative controls to assess the dynamic range of FCCS in our system. As a negative control and lower limit for binding, cells co-expressing GFP or GFP-myosin II with mCherry measured *in vivo* K_D values of 3.5 μM (**Fig. 4.2B**). In contrast, cells where GFP was directly linked to mCherry by either a 5-amino acid flexible linker or the myosin II-S1 fragment showed *in vivo* K_D values of 0.50 μM (**Fig. 4.2B**), representing positive controls, or maximum binding. We found that protein concentration did not correlate with *in vivo* K_D within our measurable range (**Fig. 4.3**). Next, we measured the *in vivo* K_D between cortexillin I and myosin II to be ~ 0.6 μM in *myoII* null and *cortI* null backgrounds, indicating their presence within the same complexes *in vivo*. Importantly, this interaction was maintained in *iqg1*, *iqg2*, and *iqg1/2* null backgrounds (*in vivo* K_D values of 0.96, 0.38, and 0.42 μM , respectively) (**Fig. 4.2C**). Thus, the cooperative mechanoresponsiveness of myosin II and cortexillin I that is

retained in an *iqg1/2* null background (Kee et al., 2012; Luo et al., 2012) is likely due to their association in these complexes, or mechanoresponsive contractility kits (MCKs). (All concentrations and binding affinity values may be found in **Table 2**.)

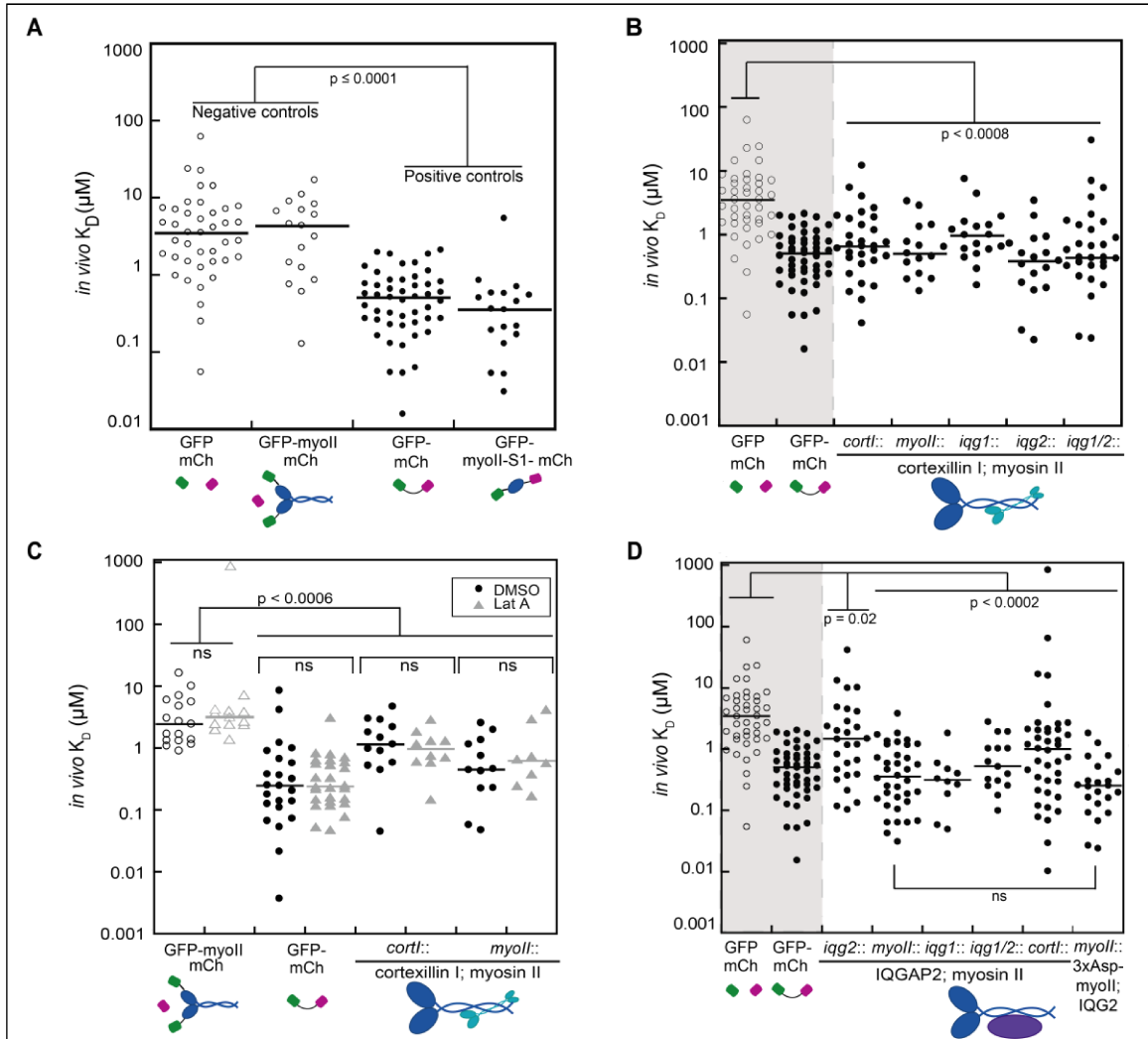
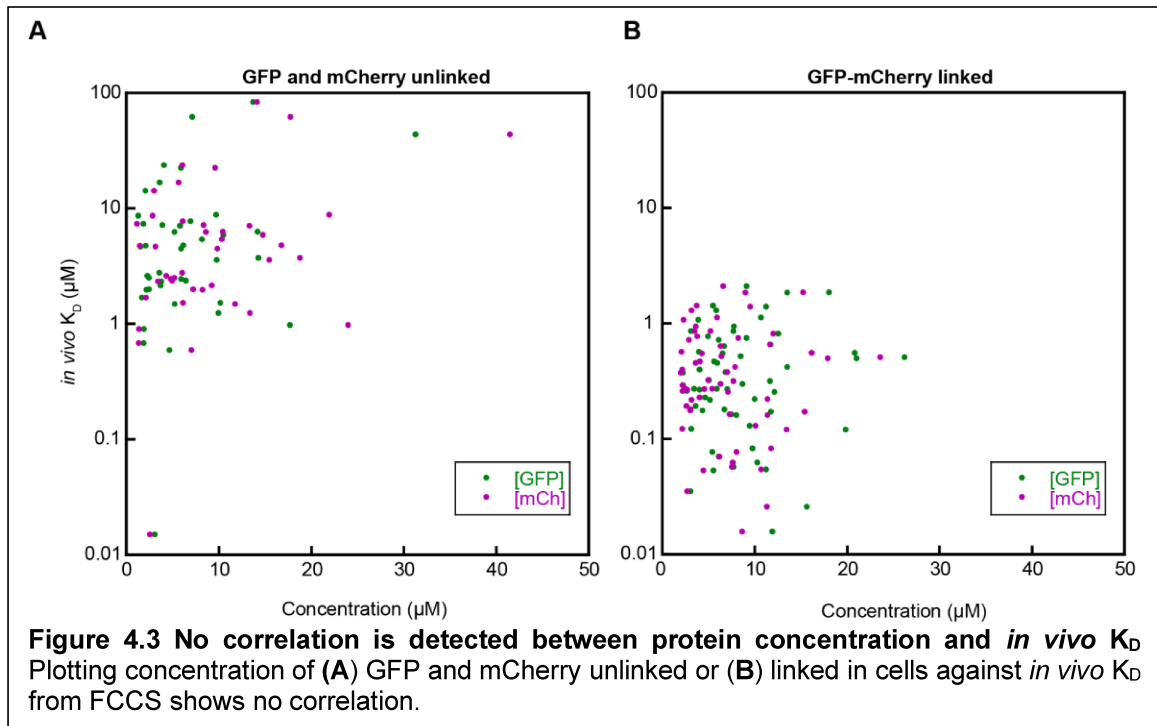


Figure 4.2. Cortexillin I and IQGAP2 interact with myosin II in the cytoplasm as detected by Fluorescence Cross-Correlation Spectroscopy (FCCS) (A) Apparent, or *in vivo*, K_D for negative and positive controls indicated. A fusion GFP-mCherry or GFP-myosin II S1-mCherry both show positive cross-correlations and apparent K_D 's in the sub- μM range. (B) FCCS detects interactions between cortexillin I and myosin II in various genetic backgrounds. (C) Treatment with 5 μM Latrunculin A does not alter the *in vivo* K_D 's between cortexillin I and myosin II. (D) IQGAP2 and myosin II also interact by FCCS. While the interaction is lost in an *iqg2* null, it is restored upon removal of IQGAP1 (*iqg1* and *iqg1/2* null). Similar *in vivo* K_D 's are measured in a *myosin II* null with either wild-type or an assembly-deficient myosin II (myosin II 3xAsp), indicating that the interaction is independent of wild-type myosin II assembly. Negative and positive controls (shaded) are reproduced from (A) for side by side comparison. Lines represent median values. P values are derived from Kruskal-Wallis followed by a Wilcoxon-Mann-Whitney test, comparing to the GFP and mCherry negative control. Open circles indicate non-interactors.



We also examined the correlation times for myosin II and cortexillin I in *cortI* and *myoII* null backgrounds to identify any changes in protein mobility with endogenous protein levels. While myosin II mobility was unchanged, cortexillin I has higher mobility (lower correlation time) in the *myoII* null background where there is unlabeled cortexillin I (Fig. 4.4A). The unlabeled cortexillin I in the *myoII* null likely competes for myosin II binding, which would result in a more mobile labeled-cortexillin I pool, thus suggesting that myosin II might be a limiting factor in the complex. Consistently, from the fluorescent particle counts, the concentrations of cortexillin are generally equal to or in slight excess of myosin II. Stoichiometric ratio differences may be further intensified as myosin II is thought to assemble into bipolar filaments through addition of dimers of myosin II functional monomers where a functional monomer is the hexamer of two heavy chains and four light chains (Luo et al., 2012; Luo and Robinson, 2015).

Since immobile proteins do not diffuse sufficiently to generate a meaningful auto-correlation signal, FCCS is unlikely to probe proteins bound to the actin network. Consistently, depolymerizing actin with Latrunculin A did not alter the cortexillin I-myosin

II *in vivo* K_D , indicating that interactions detected by FCCS are independent of the actin network (**Fig. 4.2C**). However, Latrunculin A treatment did decrease the mobility of myosin II in the *cort1* null background (**Fig. 4.4B**). If indeed more myosin II-cortexillin I complexes are formed in the *cort1* null, changing the cytoskeletal architecture of the cells may release bound complexes from the network, causing a detectable mobility shift in myosin II.

We then turned to the cortexillin-binding partner IQGAP2, which relieves IQGAP1-mediated inhibition of myosin II mechanoresponsiveness (Kee et al., 2012). We detected a positive interaction between IQGAP2 and myosin II by FCCS when complementing a *myoII* null (*in vivo* K_D of 0.36 μ M), but the interaction was much weaker in an *iqg2* null (*in vivo* K_D of 1.5 μ M) (**Fig. 4.2D**). Removing IQGAP1 from the cell restored the interaction (0.31 and 0.53 μ M in *iqg1* and *iqg1/2* nulls), implicating IQGAP1 as an inhibitor of the

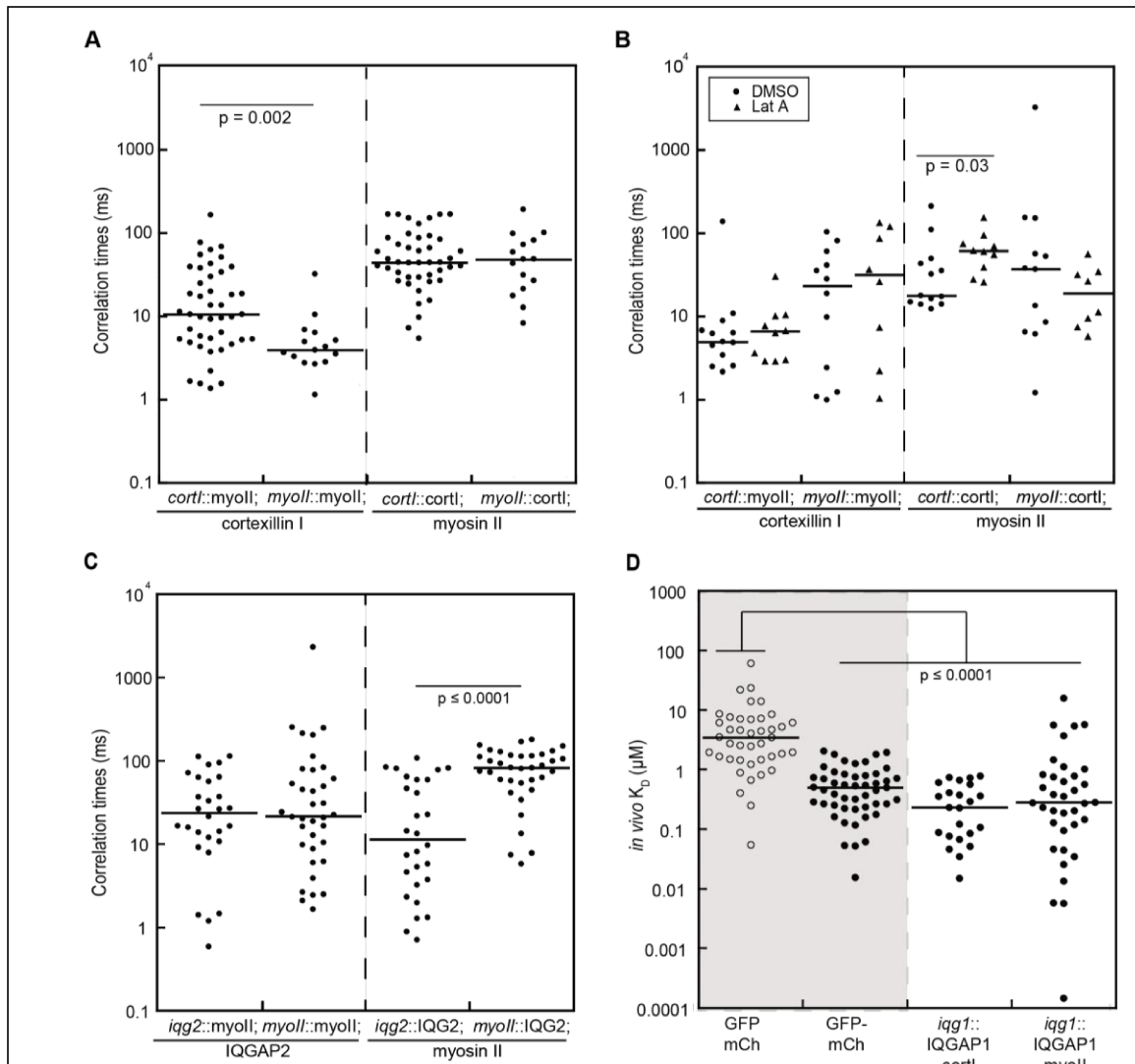


Figure 4.4. Correlation times of myosin II, cortexillin I, and IQGAP2, and *in vivo* K_D 's of IQGAP1 with myosin II and cortexillin I (A) Correlation times measured for cortexillin I and myosin II in *cortl::myosin II*; cortexillin I and *myoII::myosin II*; cortexillin I cell lines. (B) Correlation times measured for cortexillin I and myosin II in same cell lines as (A), with and without Latrunculin A treatment. (C) Correlation times measured for IQGAP2 and myosin II in *iqg2::IQGAP2*; myosin II and *myoII::IQGAP2*; myosin II. (D) Shaded region indicates FCCS controls reproduced from Fig. 4.2. IQGAP1 interacts with cortexillin I and myosin II by FCCS. Lines represent median values. P values are derived from Kruskal-Wallis followed by a Wilcoxon-Mann-Whitney test, comparing to the GFP and mCherry negative control. Negative and positive controls (shaded) are reproduced from Fig. 4.2 for side by side comparison. Open circles represent non-interactors.

IQGAP2-myosin II complex and providing a biochemical basis for antagonism of IQGAP1 on the myosin II mechanosensory system (Kee et al., 2012).

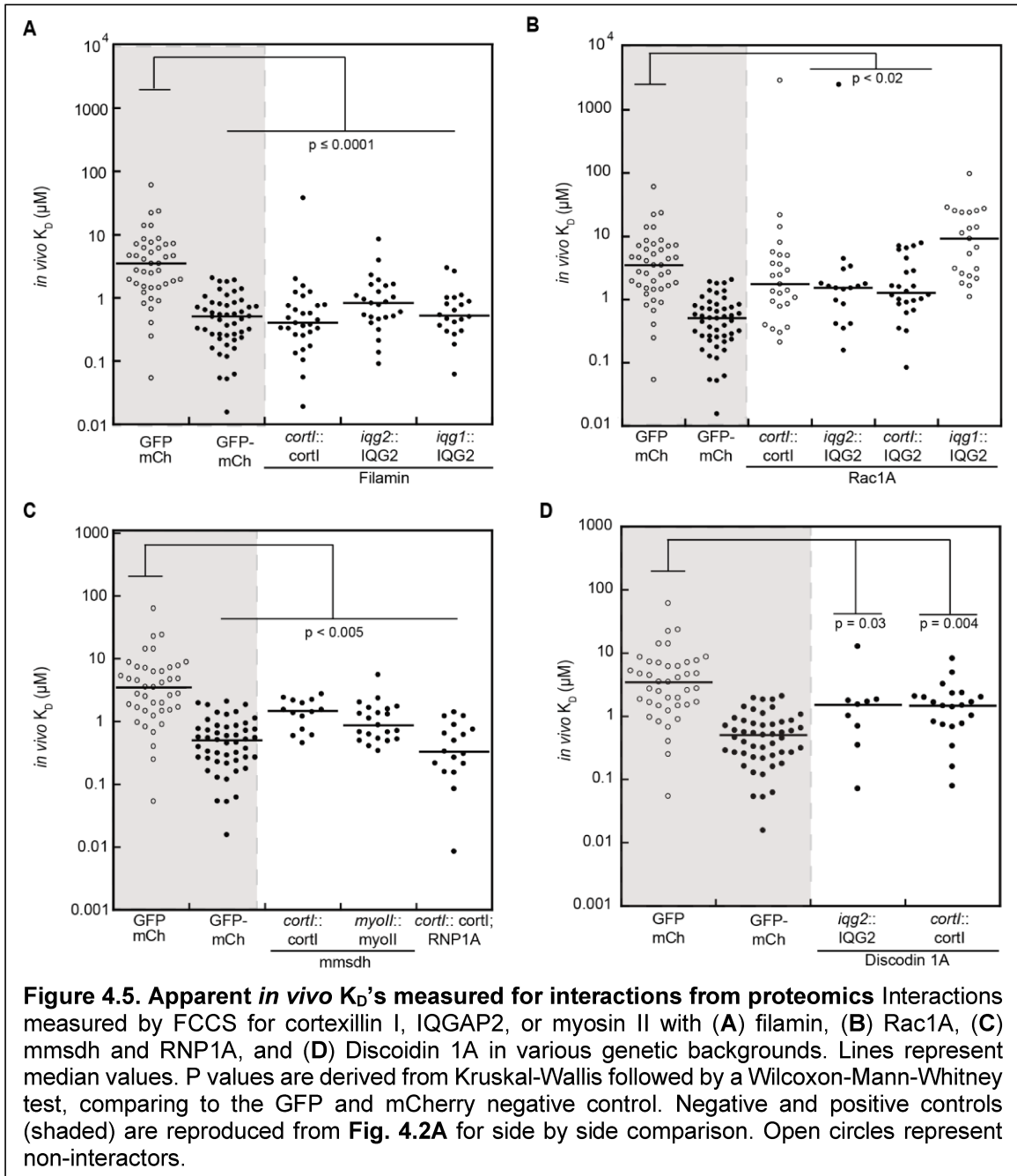
IQGAP2 and myosin II also associate in a *cortl* null (*in vivo* K_D of 0.85 μM), reproducing results detected in a *cortl//l* null by mass spectrometry (Fig. 4.2D). IQGAP2

also interacts with an assembly-deficient phosphomimetic myosin II, myosin-3xAsp, indicating that the IQGAP2-myosin II binding is independent of wild-type myosin assembly (Egelhoff et al., 1993) (**Fig. 4.2D**). The correlation times of myosin II increase upon over-expression of IQGAP2 in a *myoII* null, suggesting increased complex formation (**Fig. 4.4C**). For IQGAP1 to prevent or disassemble the IQGAP2-myosin II complexes through competition, IQGAP1 could also interact with myosin II, which we detected by FCCS (*in vivo* K_D of 0.28 μM) (**Fig. 4.4D**).

Regulatory proteins also interact with the contractility controller

In addition to characterizing the core components of the contractility controller, we also measured the binding affinities of several other interactions identified through the proteomics effort. Filamin interacted with cortexillin I and IQGAP2 as determined by FCCS (*in vivo* K_D values of 0.40 and 0.69 μM , respectively) (**Fig. 4.5A**). Although Rac1A was found to be an interactor of cortexillin I through proteomics, this interaction could not be detected by FCCS (*in vivo* K_D of 1.8 μM , not statistically significantly different from the negative control due to the width of the distribution), which could be due to the presence of both active and inactive populations of Rac1A and speaks to the sensitivity of mass spectrometry. However, IQGAP2 did weakly interact with Rac1A in a complemented *iqg2* null and a *cortI* null (*in vivo* K_D values 1.5 and 1.3 μM , respectively), but failed to interact in the absence of IQGAP1 (*in vivo* K_D of 12 μM) (**Fig. 4.5B**). Either IQGAP1 is required for the Rac1A-IQGAP2 interaction, or increased competition from myosin II or cortexillin I in the *iqg1* null prevents detection of the interaction. By FCCS, we also detected *mmsdh* interactions with cortexillin I, as suggested by mass spectrometry, and with myosin II (*in vivo* K_D values of 1.5 and 0.87 μM , respectively) (**Fig. 4.5C**). RNP-1A also interacts with cortexillin (*in vivo* K_D of 0.33 μM), and the discoidin complex subunit 1A associates with cortexillin I and IQGAP2 (*in vivo* K_D values of 1.6 and 1.5 μM , respectively) (**Fig. 4.5C,D**).

The *in vivo* biochemical confirmation of these interactions emphasizes that the combined proteomics and FCCS approach is appropriate for not only identifying the cytoskeletal proteins, but also the regulatory proteins that are likely critical for the function of the contractility controller. We next focus on deciphering the mechanism of one of the key negative regulators of the contractility controller, namely IQGAP1.



IQGAP1 inhibits the interaction between cortexillin I and IQGAP2

We used FCCS to determine whether IQGAP1 has a similar inhibitory effect on the IQGAP2-cortexillin I interaction. We found an association between IQGAP2 and cortexillin I in a complemented *cort1* null (*in vivo* K_D of 0.38 μM), and in the absence of myosin II (*in vivo* K_D of 0.21 μM), but not in the complemented *iqg2* null (*in vivo* K_D of 2.7 μM) (**Fig. 4.6A**). Competition from unlabeled cortexillin I in the *iqg2* null may prevent detection of an interaction, implicating IQGAP2 as the limiting factor for this complex. Consistently, distribution of the correlation times for cortexillin I is weakly bimodal ($p=0.045$), suggesting a population of bound and unbound protein, while correlation times for IQGAP2 increase from the *cort1* to the *iqg2* null (**Fig. 4.6B**). In addition, endogenous IQGAP1 may compete with IQGAP2 for binding cortexillin I. Consistent with this idea, removing IQGAP1 increased the binding affinity between IQGAP2 and cortexillin I by 30-fold, shifting the *in vivo* K_D to 0.12 μM in an *iqg1/2* null (**Fig. 4.6A**). Moreover, the correlation times of IQGAP2 and cortexillin I increased 7-18-fold over that seen with the *cort1* null, reflecting much larger complexes in the cytoplasm of an *iqg1/2* null (**Fig. 4.6B**). These drastic changes in affinities and correlation times were unperturbed upon treatment with Latrunculin A, indicating that the shifts are not due to interactions with the actin network or the formation of complexes sufficiently large to be restricted by the actin meshwork pore size (**Fig. 4.7A, B**). Since cortexillin I binds IQGAP1 as well (Faix et al., 2001) (**Fig. 4.4D**), to further probe the formation of the MCKs in the cytoplasm, we examined the stoichiometries of the individual interactions.

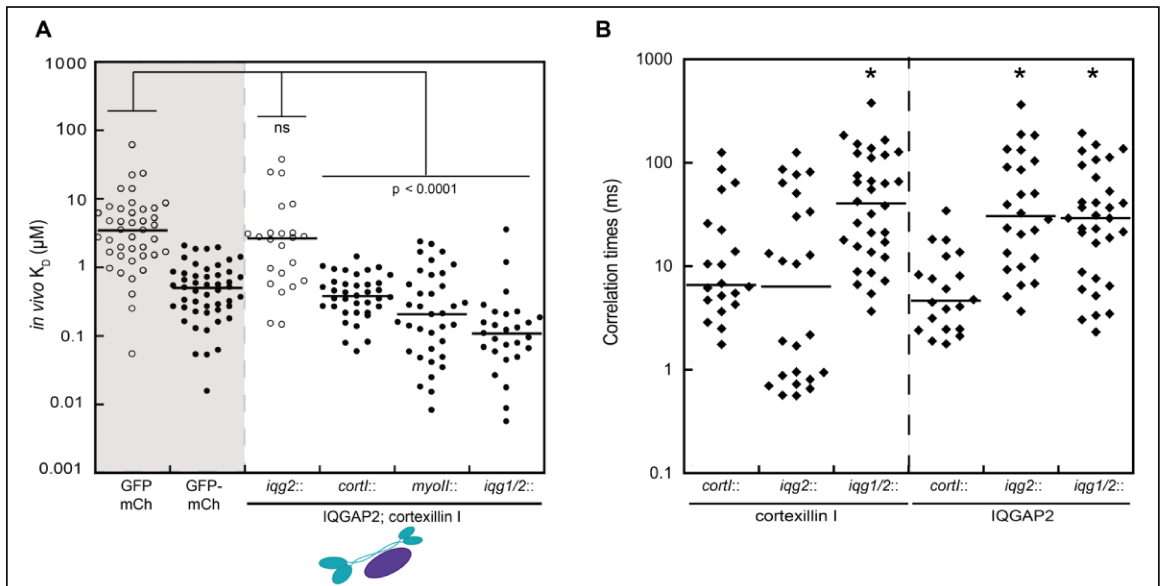
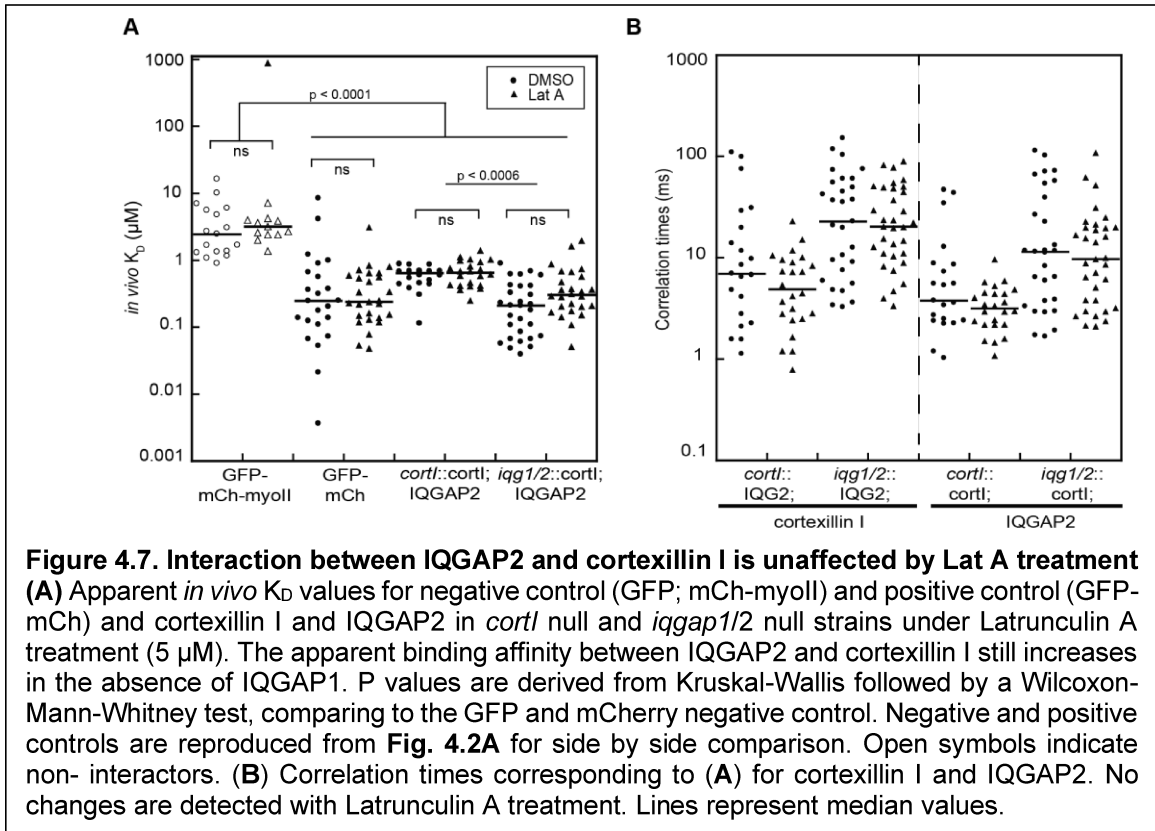


Figure 4.6. IQGAP1 inhibits the IQGAP2-cortexillin I interaction (A) FCCS measurement of *in vivo* K_D values demonstrate that IQGAP2 and cortexillin I interact in the *cortl*-null complemented background, and in the absence of myosin II. The binding is lost in the *iqg2*-null complemented cell, but the affinity between IQGAP2 and cortexillin I increases significantly in an *iqg1/2*-null. P values are derived from Kruskal–Wallis followed by a Wilcoxon–Mann–Whitney test as compared to the GFP and mCherry negative control. ns, not significant. Negative and positive controls (shaded) are reproduced from **Fig. 4.2A** for side by side comparison. **(B)** Correlation times in cell lines co-expressing labeled cortexillin I and IQGAP2. The correlation time increases for cortexillin I from the *cortl*- to *iqg1/2*-null, and increases for IQGAP2 in both the *iqg2*- and *iqg1/2*-null backgrounds, suggesting formation of larger complexes. The correlation time for cortexillin shifts to a bimodal distribution in the *iqg2*-null ($p=0.045$ by Hartigan's dip test on log-transformed data), indicating a population of bound and unbound cortexillin I caused by endogenous cortexillin I. * $P<0.001$. P values are derived from Kruskal–Wallis followed by a Wilcoxon–Mann–Whitney test as compared to the correlation time in the *cortl*-null background. Open circles indicate non-interactors. Lines represent the median values.

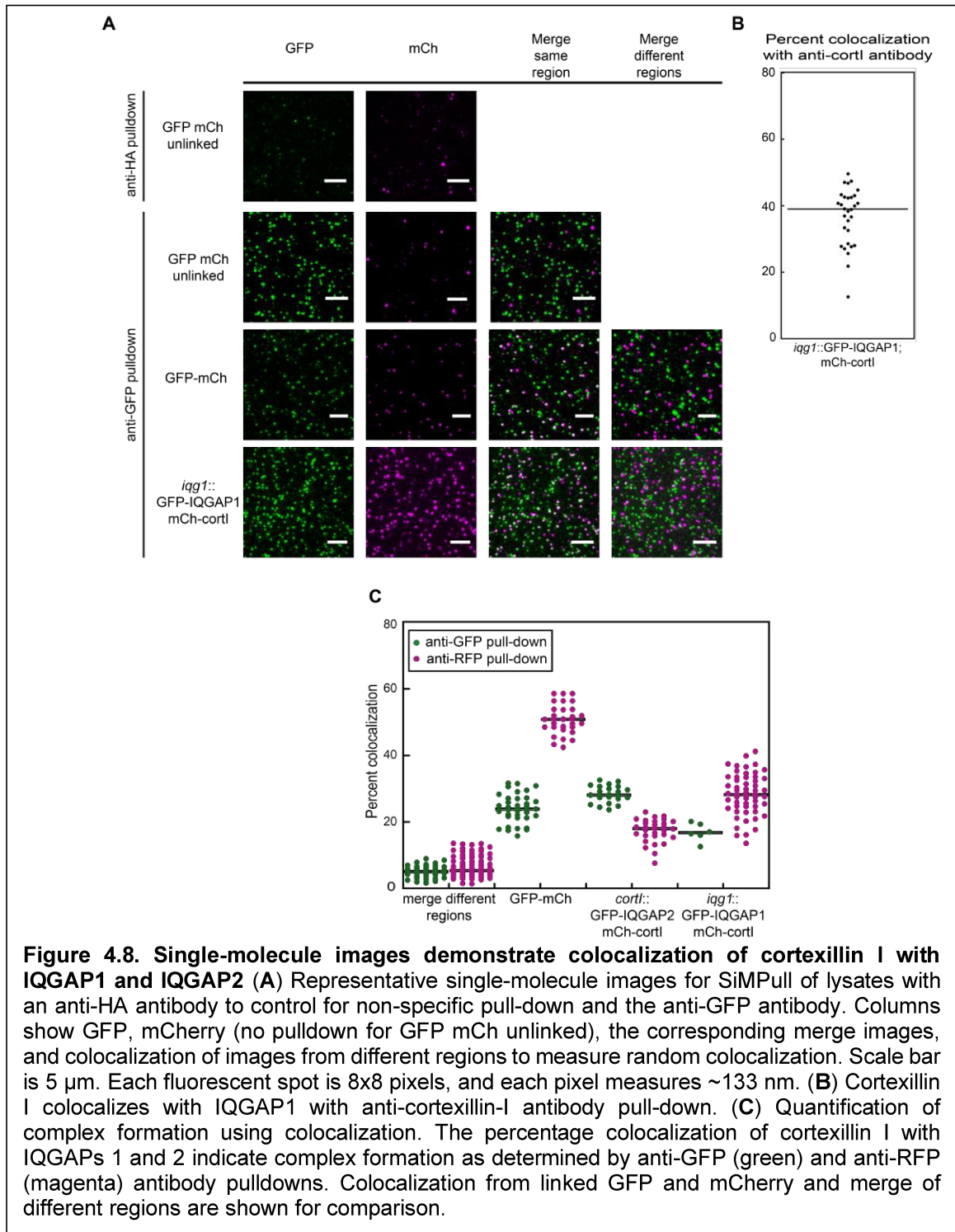


Quantifying the stoichiometries of core building blocks

We used Single-Molecule Pull-down (SiMPull) to quantify the stoichiometries of cortexillin I, IQGAP2, and IQGAP1 in these cellular complexes (Jain et al., 2011; Aggarwal and Ha, 2014). Briefly, we immunoprecipitated protein complexes containing two distinct fluorescently labelled proteins on antibody-coated slides. We visualized isolated complexes at single molecule resolution using total internal reflection fluorescence (TIRF) microscopy to quantify fluorophore colocalization (binding) and photobleaching events (oligomerization state) (Fig. 2.2). We used cells expressing GFP-mCherry (linked) and merges of different regions to determine maximum and background colocalization percentage, respectively (Fig. 4.8A). Due to incomplete maturation of GFP and mCherry, maximum colocalization is ~60% (Jain et al., 2011). Colocalization is quantified as the percentage of immunoprecipitated spots with which the opposite fluorophore co-precipitated (Fig. 4.8A). The high degree of colocalization of mCherry-cortexillin I with

GFP-IQGAP1 and GFP-IQGAP2 using antibodies against GFP, RFP, and cortexillin I further confirmed cortexillin I binding to IQGAP1 and IQGAP2 and motivated analysis of the stoichiometries of these complexes (**Fig. 4.8B,C**).

The linked and unlinked GFP and mCherry showed ~20% two-step photobleaching, while the known dimeric protein 14-3-3-GFP showed 35% two-step photobleaching. The mean-plus-two standard deviations of the linked and unlinked fluorophores was 27%, and thus, we considered 27% two-step photobleaching as a threshold whereby proteins that scored above or below this level were considered predominantly dimeric or monomeric, respectively. Based on these metrics, we conclude that both cortexillin I and IQGAP1 form complexes with two subunits each, while just a



single IQGAP2 molecule forms a complex with a cortexillin I dimer (Fig. 4.9). No events with greater than two-step photobleaching were recorded, thereby ruling out any higher order assemblies. Overall, IQGAP1 may negatively regulate mechanoresponsiveness by

sequestering away binding sites on cortexillin I, preventing the formation of the cortexillin I-IQGAP2-myosin II mechanoresponsive contractility kits.

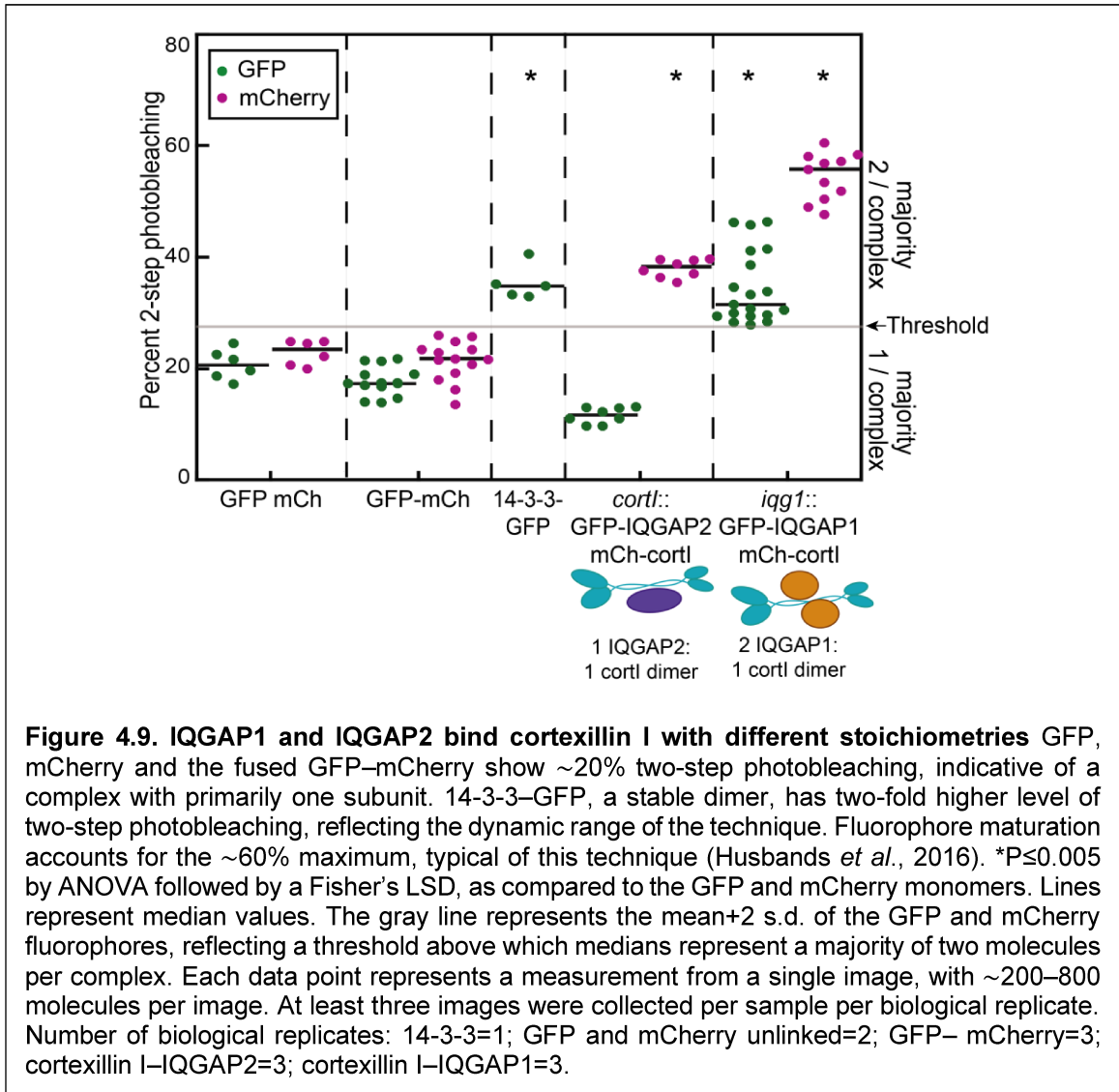


Table 2: Concentrations and *in vivo* K_D 's by FCCS

Concentrations and *in vivo* K_D 's are presented. Top row in *italics* indicates genetic background for each parameter set. Concentrations of Cortexillin I, Myosin II, IQGAP1, and Filamin are in $\mu\text{M}_{\text{dimer}}$ (in this case, when we refer to the myosin II dimer, this is the hexamer with two heavy chains and four light chains, which constitutes the functional 'monomer') while concentrations of IQGAP2, Mmsdh, RNP1A, Rac1A, and Discoidin 1A are in $\mu\text{M}_{\text{monomer}}$. Concentrations were normally distributed in real space and are listed as mean \pm s.e.m. For *in vivo* K_D 's, values were broadly distributed and nearly log normal. Therefore, in the top row, the log-space median values are provided with real space transformed medians with units in μM included in the parentheses. The log-space mean \pm s.e.m. values are provided in the bottom row.

	<i>cortl</i>		<i>myoll</i>		<i>iqg2</i>		<i>iqg1/2</i>	
	Conc.	<i>in vivo</i> K _D	Conc.	<i>in vivo</i> K _D	Conc.	<i>in vivo</i> K _D	Conc.	<i>in vivo</i> K _D
Cortexillin I	4.4 ± 0.44 μM	-0.42 (0.38 μM)	3.6 ± 0.43 μM	-0.68 (0.21 μM)	3.3 ± 0.29 μM	0.44 (2.7 μM)	5.6 ± 0.67 μM	-0.92 (0.12 μM)
IQGAP2	4.4 ± 0.43 μM	-0.43 ± 0.05	6.2 ± 0.65 μM	-0.71 ± 0.03	6.1 ± 0.69 μM	0.53 ± 0.19	6.9 ± 0.55 μM	-0.96 ± 0.11

	<i>cortl</i>		<i>myoll</i>		<i>iqg2</i>		<i>iqg1/2</i>	
	Conc.	<i>in vivo</i> K _D	Conc.	<i>in vivo</i> K _D	Conc.	<i>in vivo</i> K _D	Conc.	<i>in vivo</i> K _D
Cortexillin I	3.1 ± 0.17 μM	-0.19 (0.65 μM)	2.0 ± 0.11 μM	-0.30 (0.50 μM)	2.0 ± 0.22 μM	-0.42 (0.38 μM)	1.8 ± 0.16 μM	-0.37 (0.42 μM)
Myosin II	2.1 ± 0.11 μM	-0.17 ± 0.08	1.6 ± 0.13 μM	-0.25 ± 0.11	2.0 ± 0.28 μM	-0.48 ± 0.14	1.5 ± 0.38 μM	0.12 ± 0.33

	<i>iqg1</i>	
	Conc.	<i>in vivo</i> K _D
Cortexillin I	2.5 ± 0.21 μM	-0.23 (0.58 μM)
Myosin II	1.7 ± 0.15 μM	-0.29 ± 0.10

	<i>cortl</i>		<i>myoll</i>		<i>iqg2</i>		<i>iqg1/2</i>	
	Conc.	<i>in vivo</i> K _D	Conc.	<i>in vivo</i> K _D	Conc.	<i>in vivo</i> K _D	Conc.	<i>in vivo</i> K _D
IQGAP2	5.8 ± 0.72 μM	-0.07 (0.85 μM)	7.2 ± 0.50 μM	-0.45 (0.36 μM)	4.9 ± 0.93 μM	0.17 (1.5 μM)	8.3 ± 1.3 μM	-0.10 (0.80 μM)
Myosin II	3.6 ± 0.27 μM	0.08 ± 0.32	2.9 ± 0.25 μM	-0.46 ± 0.09	2.6 ± 0.53 μM	0.24 ± 0.17	4.4 ± 0.5 μM	-0.07 ± 0.14

	<i>iqg1</i>	
	Conc.	<i>in vivo</i> K _D
IQGAP2	6.4 ± 1.6 μM	-0.51 (0.31 μM)
Myosin II	3.3 ± 0.38 μM	-0.55 ± 0.15

	<i>iqg1</i>	
	Conc.	<i>in vivo</i> K _D
Cortexillin I	7.1 ± 0.69 μM	-0.63 (0.23 μM)
IQGAP1	5.2 ± 0.44 μM	-0.73 ± 0.10

	<i>iqg1</i>	
	Conc.	<i>in vivo</i> K _D
Myosin II	2.2 ± 0.19 μM	-0.56 (0.28 μM)
IQGAP1	3.5 ± 0.56 μM	-0.55 ± 0.08

	<i>iqg2</i>		<i>cortl</i>		<i>iqg1</i>	
	Conc.	<i>in vivo</i> K _D	Conc.	<i>in vivo</i> K _D	Conc.	<i>in vivo</i> K _D
IQGAP2	4.6 ± 0.41 μM	-0.17 (0.69 μM)	5.7 ± 0.49 μM	-0.05 (0.90 μM)	11 ± 2.1 μM	-0.43 (0.37 μM)
Filamin	1.3 ± 0.13 μM	-0.10 ± 0.11	2.1 ± 0.26 μM	-0.09 ± 0.09	2.6 ± 0.48 μM	-0.41 ± 0.13

	<i>iqg2</i>		<i>cortl</i>		<i>iqg1</i>	
	Conc.	<i>in vivo</i> K _D	Conc.	<i>in vivo</i> K _D	Conc.	<i>in vivo</i> K _D
IQGAP2	5.0 ± 0.66 μM	0.19 (1.5 μM)	7.2 ± 0.49 μM	0.11 (1.3 μM)	19 ± 2.9 μM	1.1 (12 μM)
Rac1A	5.9 ± 1.1 μM	0.26 ± 0.22	10 ± 1.1 μM	0.17 ± 0.10	6.5 ± 0.57 μM	0.98 ± 0.13

	<i>cortl</i>	
	Conc.	<i>in vivo</i> K _D
Cortexillin I	3.2 ± 0.20 μM	0.24 (1.8 μM)
Rac1A	8.3 ± 0.69 μM	0.37 ± 0.17

	<i>myo1l</i>	
	Conc.	<i>in vivo</i> K _D
Myosin II	3.6 ± 0.44 μM	-0.06 (0.87 μM)
Mmsdh	4.3 ± 1.0 μM	-0.02 ± 0.07

	<i>cortl</i>	
	Conc.	<i>in vivo</i> K _D
Cortexillin I	4.3 ± 0.53 μM	0.17 (1.5 μM)
Mmsdh	3.4 ± 0.87 μM	0.11 ± 0.07

	<i>cortl</i>	
	Conc.	<i>in vivo</i> K _D
Cortexillin I	3.7 ± 0.26 μM	0.17 (1.5 μM)
Discoidin 1A	5.9 ± 0.78 μM	0.08 ± 0.10

	<i>iqg2</i>	
	Conc.	<i>in vivo</i> K _D
IQGAP2	10.9 ± 2.0 μM	0.18 (1.5 μM)
Discoidin 1A	10.1 ± 1.9 μM	0.03 ± 0.20

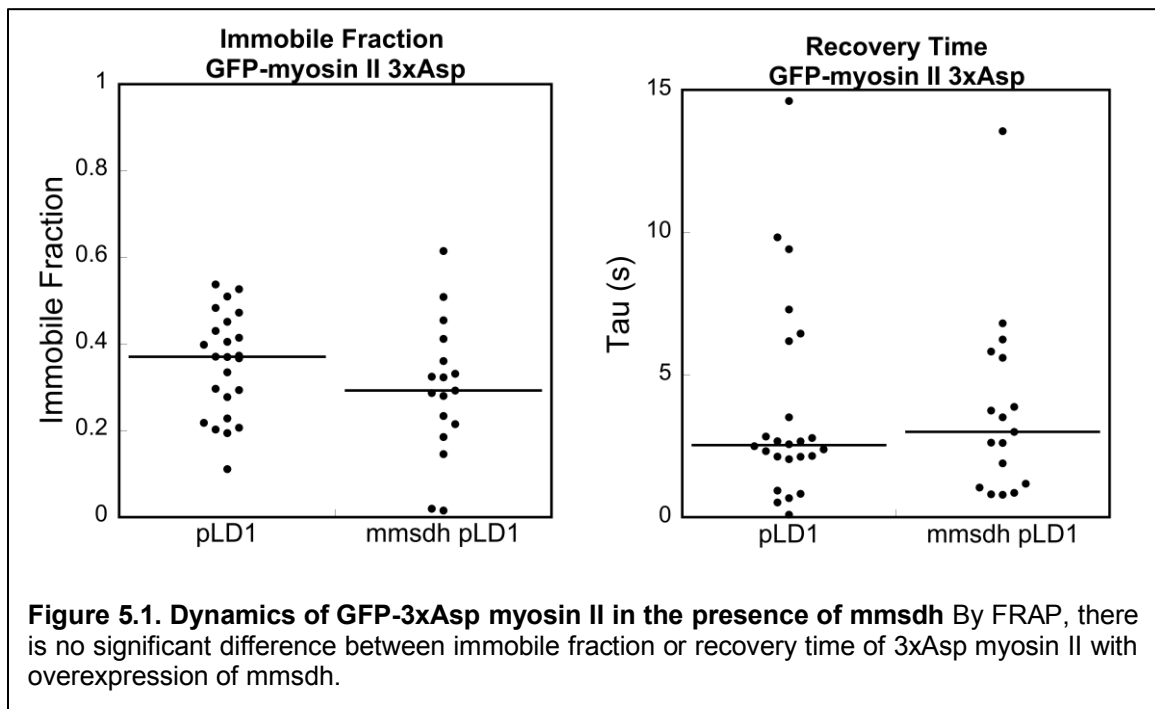
Chapter 5 Uncovering the role of mmsdh in the contractility controller

The proteomics analysis identified methylmalonate-semialdehyde dehydrogenase (mmsdh) as an interactor of cortexillin I. Mmsdh catalyzes the production of propionyl- and acetyl-coA from coenzyme A and substrates from valine degradation. The potential interaction between mmsdh and cortexillin I is particularly exciting because overexpression of mmsdh suppresses the dominant-negative phenotype of a myosin II phosphomimetic in *Dictyostelium* (Ren et al., 2014). Phosphorylation of three key threonines in the tail region of myosin II significantly reduces assembly of bipolar filaments. A phosphomimetic, 3xAsp-myosin II, fails to accumulate at the cleavage furrow in *myoII* null cells, and in a wild-type background, inhibits growth of *Dictyostelium* in suspension culture (a highly restrictive growth condition for cells with impaired cytokinesis). Mmsdh overexpression partially rescued suspension growth and promoted GFP-3xAsp-myosin II accumulation at the cleavage furrow of *myoII* null cells (Ren et al., 2014). Further, detecting positive cross-correlations between mmsdh and both myosin II and cortexillin I by FCCS also suggests a biochemical interaction between these proteins (Kothari et al., 2019b). Interestingly, myosin II has been shown to be acetylated during mitosis in mitotic cells (Chuang et al., 2010). Moreover, imposing mechanical stress on rat sarcomeres increases the acetylation of cardiac myosin II, increasing myosin's actin-binding affinity and power output (Samant et al., 2015).

Therefore, it is possible that myosin II and other cytoskeletal proteins are modified by propionylation as well. Histone acetyltransferases PCAF and p300 use propionyl-coA as a substrate *in vitro*, and histone deacetylase Sir2 removes the modification (Liu et al., 2009; Choudhary et al., 2014; Kaczmarek et al., 2017). Histones and p53 are both known to be propionylated *in vivo*, although little is known about this PTM's role in regulation or what other propionylated proteins may exist (Liu et al., 2009). We hypothesize that

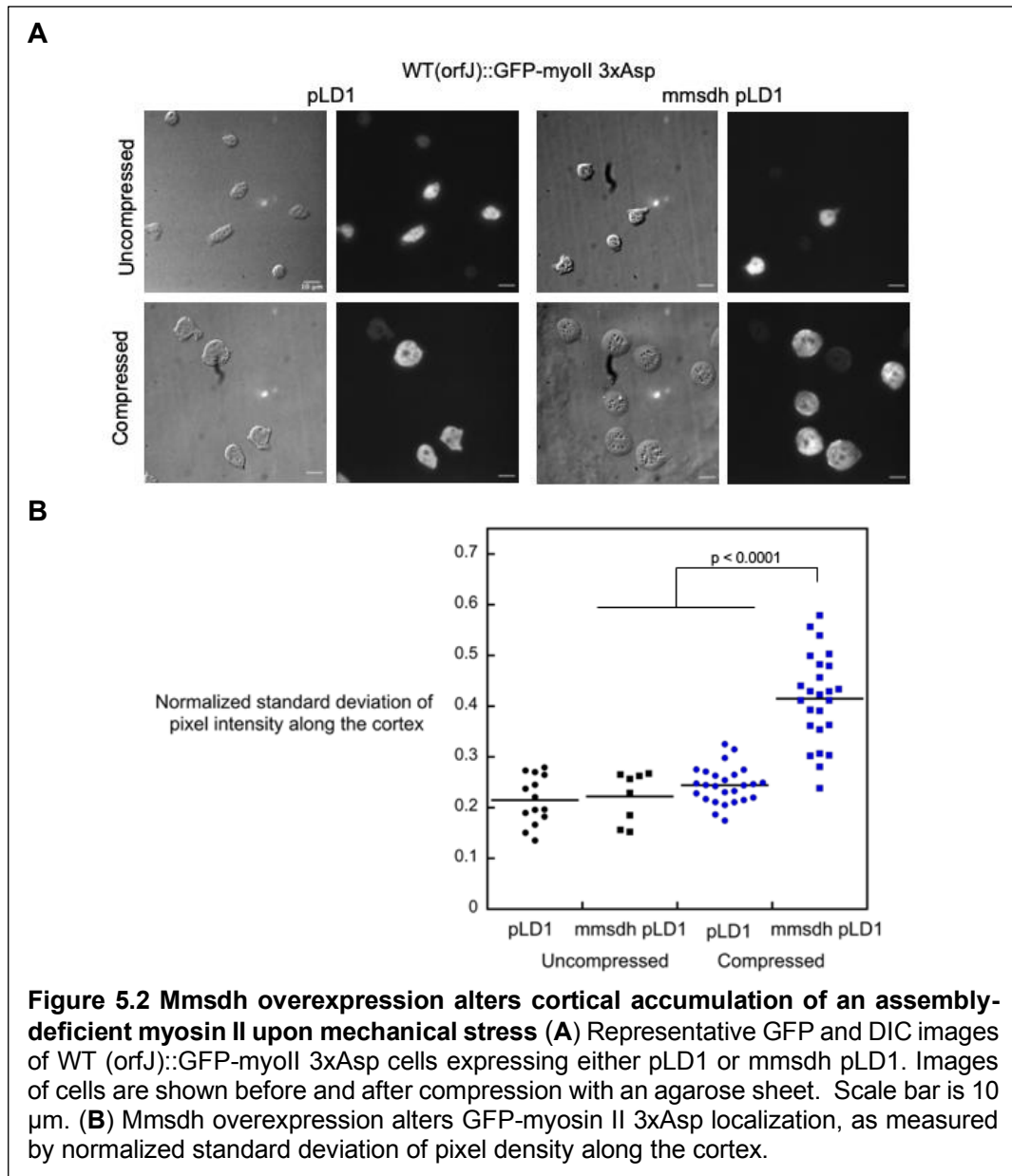
propionylation is a post-translational modification that regulates the load-dependent activity of myosin II, and potentially other proteins in the control system. Overexpression of *mmsdh*, which rescues the phosphomimetic 3xAsp-myosin II phenotype, could generate a larger pool of propionyl-CoA, which may lead to increased modification of cytoskeletal proteins and facilitate positive regulation of the mechanosensory system.

To characterize the role of *mmsdh* in the contractility controller, we first explored whether 3xAsp myosin II dynamics were altered after overexpression of *mmsdh*. We generated WT (*Ax3(Replicase orf+)*, a.k.a. *orfJ*) cells co-expressing GFP-myosin II 3xAsp with either a vector control or overexpressing *mmsdh*. By Fluorescence Recovery After Photobleaching (FRAP), we did not detect any change in the immobile fraction or recovery time of myosin II 3xAsp (**Fig. 5.1**).



Since the mutant myosin II had been shown to accumulate at the furrow of dividing *myoII* null cells, we wondered whether this was specific to load sensing or required chemical signaling during cytokinesis. We used the same cell lines generated above to perform the agarose compression assay to test whether 3xAsp would respond to global

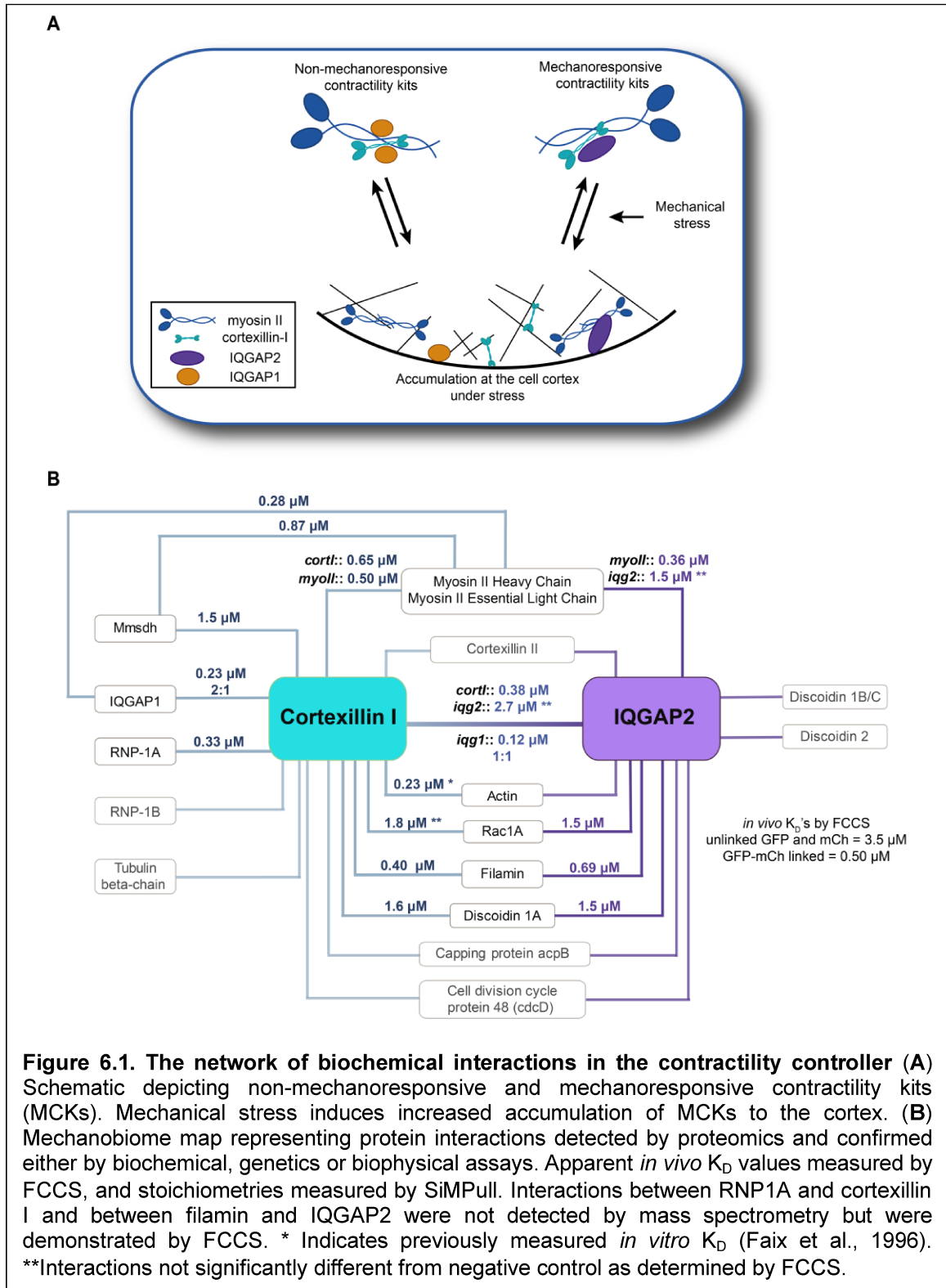
compression to the cells, as wild-type myosin II does. Interestingly, with the overexpression of *mmsdh*, we measured an increase in the coarseness index, or the standard deviation of the pixel intensity of GFP-myosin II 3xAsp cortical localization under global compression (**Fig. 5.2**). These data suggest that *mmsdh* may alter filament assembly or myosin II actin-binding affinity specifically under load.



Chapter 6 Conclusions

At this point, we have recognized that the contractile system is structured as a control system composed of feedback and tunable setpoints. The purpose of such a system is to respond quickly to disturbances (inputs), thereby returning the system to its setpoint. This then begs the question as to how large molecular assemblies can be built on the 10-100 seconds time-scale. The answer appears to lie in preformed complexes that exist in an equilibrium before their activation by spatial and temporal signals.

Here, we built from an unbiased mass spectrometry analysis to highlight previously unappreciated components of the mechanobiome and to characterize the biochemical interactions that drive the contractility controller (**Fig. 6.1A,B**). The combination of proteomics and quantitative *in vivo* biochemical analysis indicates that myosin II and cortexillin I form complexes in the cytoplasm, providing a biochemical basis for their cooperative mechanoaccumulation (Luo et al., 2012). The IQGAPs also bind the cortexillin I-myosin II complexes, providing key regulation of these mechanoresponsive proteins. Although myosin II has not been shown to interact biochemically with cortexillin I or IQGAP2 in *Dictyostelium* previously, myosin II has been shown to bind the IQGAP2 paralog, Rng2, in *Schizosaccharomyces pombe* (Laporte et al., 2011; Laplante et al., 2016). Moreover, mammalian IQGAP1 interacts with non-muscle myosin II essential light chain through its IQ motif *in vitro* (Weissbach et al., 1998) (although it should be noted that the *Dictyostelium* IQGAPs do not contain the IQ motif). Thus, the ability of IQGAPs to interact with myosin II proteins appears to be a highly conserved function, spanning a billion years of evolution. Perhaps it is of no surprise then that IQGAPs provide such an essential role in the contractility controller.



The cortexillin I-IQGAP2-myosin II complexes appear to be the functional unit of these proteins that then engages with the cytoskeletal network. In fact, the concept that

proteins pre-form into complexes in the cytoplasm has precedence. Myosin II, for example, exists in the cytoplasm as a functional hexamer, with two essential and two regulatory light chains bound to a dimeric heavy chain. It would be impractical for the cell to mount a response to a mechanical stress input, which propagates on the timescale of sub-to low numbers of seconds, if it had to assemble each heavy chain and light chain independently. Scaling up, the cell appears to use this same strategy of utilizing pre-assembled complexes by creating kits of cortexillin I-IQGAP2-myosin II (MCKs), which are then primed to be rapidly activated when the appropriate chemical or mechanical stimulus is experienced (**Fig. 6.1A**).

To ensure that the system it is not overly mechanosensitive, IQGAP1 serves as a competitive inhibitor of IQGAP2 for cortexillin I and myosin II. While IQGAP1 is thought to bind cortexillin I's C-terminal domain and IQGAP2 binds cortexillin's N-terminal domain, it is possible that interactions with two IQGAP1 molecules occlude the binding sites on cortexillin I for IQGAP2 (Faix et al., 2001; Mondal et al., 2010). IQGAP1 also impedes the formation or promotes the disassembly of the MCKs to create a population of free, unbound IQGAP2 monomers thereby attenuating the sensitivity of the controller. Moreover, interactions between cortexillin I, IQGAP2, activated Rac1A, and filamin provide further spatial and temporal regulation of the controller (Faix et al., 2001; Mondal et al., 2010).

Precedence for this idea of complex assembly also exists in *Schizosaccharomyces pombe* where pre-cursor nodes are used to build the cytokinetic ring. Careful concentration measurements and super-resolution imaging of key cytokinetic proteins indicate that pre-cursor structures form during mitotic entry, which are regulated by mitotic kinases, such as Cdr1p and Cdr2p (Vavylonis et al., 2008; Akamatsu et al., 2014; Akamatsu et al., 2017). Upon mitotic entry, the sequential addition of Mid1 (anillin), Myo2 heavy and light chains, and Rng2 (IQGAP2) forms the nodes that then coalesce along the

equatorial region to build the cytokinetic ring (Wu and Pollard, 2005; Akamatsu et al., 2014). Interestingly, these nodes initially form during interphase and coalesce to drive ring constriction. Their presence in interphase suggests the potential for functions beyond cytokinesis as well (Martin and Berthelot-Grosjean, 2009; Moseley et al., 2009; Akamatsu et al., 2014). While these MCKs appear to be critical during mechanoresponse in interphase cells, it is likely they are also the components that build the cytoskeletal meshwork at the equatorial region during cytokinesis to drive furrow ingression. This raises the intriguing question of whether these kits are functionally similar to the relatively stable cytokinetic nodes in fission yeast. It is possible that these stable assemblies (with minute-time-scale dynamics) appear within the lower concentrations of actin and cytokinetic proteins present in yeast, whereas much faster dynamics (on a time-scale of seconds) are at play in *Dictyostelium* where their concentrations are also much higher (Wu and Pollard, 2005; Laporte et al., 2011; Robinson et al., 2012; Srivastava and Robinson, 2015).

In the textbook model, cytokinesis is a process driven by the contractile actomyosin ring that forms at the cleavage furrow. However, a number of studies have revealed that a complex meshwork of actin filaments, myosin II bipolar filaments, actin cross-linkers, and regulatory proteins promotes accurate cleavage furrow ingression, actively tuning the protein amounts and mechanical properties (power output, viscoelasticity, and strain stiffening) of the contractile machinery in *Dictyostelium* (Effler et al., 2006; Reichl et al., 2008b; Kee et al., 2012; Luo et al., 2012; Srivastava and Robinson, 2015), *Caenorhabditis elegans* (Descovich et al., 2018), and mammalian systems (Manukyan et al., 2015; Schiffhauer et al., 2016). Our work reveals key biochemical interactions that are critical for the contractility controller and emphasizes that the mechanobiome is composed of more than just actin-binding cytoskeletal proteins.

Detecting interactions between the contractility controller and several unexpected proteins by proteomics and FCCS suggests that the mechanobiome consists of a network of proteins that integrates feedback from various seemingly unrelated processes (**Fig. 6.1B**). For example, *mmsdh* may facilitate feedback between metabolism, nutrient sensing, and cell mechanics, and such cross talk between these fundamental cellular mechanisms has been uncovered in other systems (Bays et al., 2017; Hamann et al., 2017). Since the RNP-1A was initially discovered in a genetic suppression of nocodazole, these RNPs may provide cross-talk between microtubules and the actin cytoskeletal network (Zhou et al., 2010; Ngo et al., 2016). The discoidins, which are traditionally considered lectins, may link the plasma membrane to the cytoskeletal network. The presence of these proteins in the mechanobiome reveals that the contractility controller does not function in isolation, but rather in concert with various cellular processes. Our work has demonstrated that multiple regulatory features of the mechanobiome are crucial for allowing the cell to robustly adapt to its changing environment.

The myosin II machinery, which includes actin, myosin II and actin crosslinkers, can no longer be viewed as a merely passive, downstream effector of upstream signal transduction networks. Contractility, often considered the main function of myosin II, is only one of its many roles. In reality, myosin II contributes in at least eight different ways to cell function: cortical tension, viscoelasticity, fluidization, mechanoreponse, membrane-cortex attachment, adhesion, feedback, in addition to contractility. More accurately, the myosin II network is a sophisticated integrator of mechanical and biochemical signaling inputs that continuously 'senses' and 'monitors' its status by using its control system structure in order to promote cell- and tissue-level morphogenetic processes. Furthermore, the myosin II contractile machinery communicates and integrates these inputs into changes on the longer-time-scale that are induced by directing the gene expression and metabolic profiles. In addition, many components identified in

the control systems include elements that feed into signaling, growth, and cell identity pathways. While it is necessary to consider the broader concepts of genomics and epigenetics, proteomics and metabolomics, investigating the role the mechanobiome plays in integrating these 'omics' to drive the behavior of cells, tissue, and ultimately organisms will be essential.

Chapter 7 Future Directions

In the future, there are many directions in which this study could progress. Here, I have focused on identifying and measuring the biochemical interactions of the contractility controller in live cells. It would be interesting to determine whether these interactions of the mechanoresponsive contractility kits exist *in vitro*. An *in vitro* sedimentation assay with purified cortexillin I and a myosin II tail fragment did not show any interaction, although the dynamic range for the technique is limited (data not shown). Purification of the components (myosin II, cortexillin I, IQGAP1, and IQGAP2) and measurements of binding affinities, changes in myosin II bipolar thick filament assembly, and binding affinities under load in an optical trap could yield insight into whether there is direct competition between the IQGAPs for binding myosin II and cortexillin I. Measuring changes under load could also inform the molecular mechanisms behind the cooperative mechanoresponsive behavior of myosin II and cortexillin I. Identifying the direct interactors could also help us understand the mechanisms of formation of the MCKs and the balance between the mechanoresponsive and non-mechanoresponsive populations.

Further, determining whether the MCK concept holds true in mammalian cells will be crucial. Many recent reports have shown the importance of complex assemblies in the cytoplasm (as mentioned above) and understanding the role of these MCKs could be critical for understanding the contractility controller in mammalian cells. Since IQGAP1 and anillin, which we consider to be the functional homolog of cortexillin I, have been shown to bind myosin II, it is possible that these proteins form cytoplasmic complexes in mammalian cells as well (Weissbach et al., 1998; Straight et al., 2005). As the actomyosin dynamics are slightly different between *Dictyostelium* and mammalian cells, mammalian cells may not require the same complex formation for rapid accumulation under stress. In addition, while we can study all the conserved proteins between *Dictyostelium* and

mammalian systems, an unbiased mass spectrometry approach could identify additional components that are required. For example, the BioID proximity-dependent labeling approach could be used to identify differential protein-protein interactions in the presence or absence of stress, perhaps through global agarose compression. Identifying the key players could provide greater insight into the molecular mechanisms that drive the contractility controller in mammalian cells. It would also be informative to determine whether there are alterations in the protein complexes in normal versus disease states, and across different cell lines. Evidence suggests that IQGAP1 may act as an oncogene, whereas IQGAP2 may act as a tumor suppressor (White et al., 2009). These IQGAPs have been shown to interact with a number of proteins in different signaling pathways, and thus their roles in tumorigenesis may be the result of activation of these growth pathways. It is also possible that if IQGAPs similarly regulate components of the mechanobiome, these protein-protein interactions could play a role in tumor progression.

Studying the functions of the “unusual suspects” that were identified both through the proteomics and genetic suppression selections will shed light on the feedback between mechanics and gene regulation, glycobiology, and metabolism. The RNA-binding proteins (RNPs), discoidins, and mmsdh have all been shown to contribute to the mechanobiome through multiple distinct approaches. Mmsdh, which we have shown interacts with both cortexillin I and myosin II by FCCS, could potentially play a role in regulating MCKs. Performing the genetic suppression selection of the assembly-deficient myosin II (myoII-3xAsp) with the catalytically dead mutant of mmsdh will be critical in determining whether the catalytic activity of mmsdh is required for rescuing the phenotype. This would point to a potential metabolic role and perhaps a post-translational modification such as propionylation that could impact myosin II function. Specific sites of proteins that are propionylated could be identified by mass spectrometry, and further mutational analysis could inform on the function of the post-translational modification. If the catalytic activity

is not important for the function of mmsdh in the contractility controller, mmsdh may act as a scaffold for the MCKs or alter certain protein-protein interactions. These “unusual suspects” could be integral to the mechanoresponsive system, and it is possible that, once again, alteration in regulation of these proteins in normal versus disease states could generate insight into disease progression and potential therapeutic options.

The impact of fusing control theory with the concepts of the mechanobiome has a wide range of benefits. Not only does this integration provide a framework for understanding how cells, and ultimately tissues, function, it provides the next generation of entry points for creating optimal therapeutic interventions. For example, one might want to pharmacologically target a key component, e.g. a non-muscle myosin II, to treat cancer (Surcel et al., 2015; Wong et al., 2015; Picariello et al., 2019; Surcel and Robinson, 2019). However, if the system is shifted one way or the other relative to the system’s setpoint optimum, it would be possible to erroneously shift the system so that the disease scenario is exacerbated instead of corrected or improved. Another potential application might be found in cell engineering strategies. Cellular behaviors might be able to be engineered more precisely if it is understood where the system is poised and in which direction it should be shifted. Finally, we hope to encourage broadening our tendency to consider linear pathways by incorporating the universal principles of control theory to create a truly systems-level understanding of biology.

Contributions

Vasudha Srivastava, a former graduate student in the lab, set up the initial study by conducting the proteomics analysis with Irina Tchernyshyov and Jennifer E. Van Eyk. The Single Molecule Pulldown studies were completed in collaboration with Vasudha Aggarwal and Taekjip Ha at Hopkins. The agarose compression with overexpression of mmsdh was performed by Nan Zhang, a rotation student in the lab. The illustration of the cortex (**Fig. 1.1**) was completed by Art as Applied to Medicine student Cecilia Johnson.

This work was supported by the National Institutes of Health (R01GM66817 to Douglas N. Robinson, F31GM122258 to Priyanka Kothari, T32GM007445 to BCMB Graduate Program) and the Defense Advanced Research Projects Agency (HR0011-16-C-0139; Pablo A. Iglesias and Douglas N. Robinson).

Bibliography

Aggarwal, V. and Ha, T. (2014). Single-molecule pull-down (SiMPull) for new-age biochemistry: methodology and biochemical applications of single-molecule pull-down (SiMPull) for probing biomolecular interactions in crude cell extracts. *Bioessays* **36**, 1109-1119.

Akamatsu, M., Berro, J., Pu, K. M., Tebbs, I. R. and Pollard, T. D. (2014). Cytokinetic nodes in fission yeast arise from two distinct types of nodes that merge during interphase. *J. Cell Biol.* **204**, 977-988.

Akamatsu, M., Lin, Y., Bewersdorf, J. and Pollard, T. D. (2017). Analysis of interphase node proteins in fission yeast by quantitative and superresolution fluorescence microscopy. *Mol. Biol. Cell* **28**, 3203-3214.

Bacia, K., Kim, S. A. and Schwille, P. (2006). Fluorescence cross-correlation spectroscopy in living cells. *Nat. Methods* **3**, 83-89.

Bacia, K. and Schwille, P. (2007). Practical guidelines for dual-color fluorescence cross-correlation spectroscopy. *Nat. Protoc.* **2**, 2842-2856.

Bai, H., Zhu, Q., Surcel, A., Luo, T., Ren, Y., Guan, B., Liu, Y., Wu, N., Joseph, N. E., Wang, T. L. et al. (2016). Yes-associated protein impacts adherens junction assembly through regulating actin cytoskeleton organization. *Am. J. Physiol. Gastrointest. Liver Physiol.* **311**, G396-G411.

Bays, J. L., Campbell, H. K., Heidema, C., Sebbagh, M. and DeMali, K. A. (2017). Linking E-cadherin mechanotransduction to cell metabolism through force-mediated activation of AMPK. *Nat. Cell Biol.* **19**, 724-731.

Beck, H., Flynn, K., Lindenberg, K. S., Schwarz, H., Bradke, F., Di Giovanni, S. and Knoll, B. (2012). Serum Response Factor (SRF)-cofilin-actin signaling axis modulates mitochondrial dynamics. *Proc. Natl. Acad. Sci. USA* **109**, E2523-2532.

Bement, W. M., Leda, M., Moe, A. M., Kita, A. M., Larson, M. E., Golding, A. E., Pfeuti, C., Su, K. C., Miller, A. L., Goryachev, A. B. et al. (2015). Activator-inhibitor coupling between Rho signalling and actin assembly makes the cell cortex an excitable medium. *Nat. Cell Biol.* **17**, 1471-83.

Bierbaum, M. and Bastiaens, P. I. (2013). Cell cycle-dependent binding modes of the ran exchange factor RCC1 to chromatin. *Biophys. J.* **104**, 1642-1651.

Blanchoin, L., Boujemaa-Paterski, R., Sykes, C. and Plastino, J. (2014). Actin dynamics, architecture, and mechanics in cell motility. *Physiol. Rev.* **94**, 235-263.

Broders-Bondon, F., Nguyen Ho-Boulidoires, T. H., Fernandez-Sanchez, M. E. and Farge, E. (2018). Mechanotransduction in tumor progression: The dark side of the force. *J. Cell Biol.* **217**, 1571-1587.

Bulsecq, D. A. and Wolf, D. E. (2013). Fluorescence correlation spectroscopy: molecular complexing in solution and in living cells. *Methods Cell Biol.* **114**, 489-524.

Caino, M. C., Ghosh, J. C., Chae, Y. C., Vaira, V., Rivadeneira, D. B., Favarsani, A., Rampini, P., Kossenkov, A. V., Aird, K. M., Zhang, R. et al. (2015). PI3K therapy reprograms mitochondrial trafficking to fuel tumor cell invasion. *Proc. Natl. Acad. Sci. USA* **112**, 8638-8643.

Chan, C. E. and Odde, D. J. (2008). Traction dynamics of filopodia on compliant substrates. *Science* **322**, 1687-1691.

Chang, L., Azzolin, L., Di Biagio, D., Zanconato, F., Battilana, G., Lucon Xiccato, R., Aragona, M., Giulitti, S., Panciera, T., Gandin, A. et al. (2018). The SWI/SNF complex is a mechanoregulated inhibitor of YAP and TAZ. *Nature* **563**, 265-269.

Charras, G. and Yap, A. S. (2018). Tensile Forces and Mechanotransduction at Cell-Cell Junctions. *Curr. Biol.* **28**, R445-R457.

Chen, T., Saw, T. B., Mege, R. M. and Ladoux, B. (2018). Mechanical forces in cell monolayers. *J. Cell Sci.* **131**, 1-11.

Choudhary, C., Weinert, B. T., Nishida, Y., Verdin, E. and Mann, M. (2014). The growing landscape of lysine acetylation links metabolism and cell signalling. *Nat. Rev. Mol. Cell Biol.* **15**, 536-50.

Chuang, C., Lin, S. H., Huang, F., Pan, J., Josic, D. and Yu-Lee, L. Y. (2010). Acetylation of RNA processing proteins and cell cycle proteins in mitosis. *J. Proteome Res.* **9**, 4554-64.

Chugh, P. and Paluch, E. K. (2018). The actin cortex at a glance. *J. Cell Sci.* **131**, 1-9.

Clark, A. G., Dierkes, K. and Paluch, E. K. (2013). Monitoring actin cortex thickness in live cells. *Biophys. J.* **105**, 570-580.

Condeelis, J., Vahey, M., Carboni, J. M., DeMey, J. and Ogiwara, S. (1984). Properties of the 120,000- and 95,000-dalton actin-binding proteins from Dictyostelium discoideum and their possible functions in assembling the cytoplasmic matrix. *J. Cell Biol.* **99**, 119s-126s.

Cunniff, B., McKenzie, A. J., Heintz, N. H. and Howe, A. K. (2016). AMPK activity regulates trafficking of mitochondria to the leading edge during cell migration and matrix invasion. *Mol. Biol. Cell* **27**, 2662-2674.

Descovich, C. P., Cortes, D. B., Ryan, S., Nash, J., Zhang, L., Maddox, P. S., Nedelec, F. and Maddox, A. S. (2018). Cross-linkers both drive and brake cytoskeletal remodeling and furrowing in cytokinesis. *Mol. Biol. Cell* **29**, 622-631.

Dickinson, D. J., Robinson, D. N., Nelson, W. J. and Weis, W. I. (2012). alpha-catenin and IQGAP regulate myosin localization to control epithelial tube morphogenesis in Dictyostelium. *Dev. Cell* **23**, 533-546.

Dogterom, M. and Koenderink, G. H. (2019). Actin-microtubule crosstalk in cell biology. *Nat. Rev. Mol. Cell Biol.* **20**, 38-54.

Duan, R., Kim, J. H., Shilagardi, K., Schiffhauer, E. S., Lee, D. M., Son, S., Li, S., Thomas, C., Luo, T., Fletcher, D. A. et al. (2018). Spectrin is a mechanoresponsive protein shaping fusogenic synapse architecture during myoblast fusion. *Nat. Cell Biol.* **20**, 688-698.

Dupont, S., Morsut, L., Aragona, M., Enzo, E., Giulitti, S., Cordenonsi, M., Zanconato, F., Le Digabel, J., Forcato, M., Bicciato, S. et al. (2011). Role of YAP/TAZ in mechanotransduction. *Nature* **474**, 179-183.

Effler, J. C., Kee, Y.-S., Berk, J. M., Tran, M. N., Iglesias, P. A. and Robinson, D. N. (2006). Mitosis-specific mechanosensing and contractile protein redistribution control cell shape. *Curr. Biol.* **16**, 1962-1967.

Egelhoff, T. T., Lee, R. J. and Spudich, J. A. (1993). *Dictyostelium* myosin heavy chain phosphorylation sites regulate myosin filament assembly and localization *in vivo*. *Cell* **75**, 363-371.

Engler, A. J., Sen, S., Sweeney, H. L. and Discher, D. E. (2006). Matrix elasticity directs stem cell lineage specification. *Cell* **126**, 677-689.

Faix, J., Clougherty, C., Konzok, A., Mintert, U., Murphy, J., Albrecht, R., Muhlbauer, B. and Kuhlmann, J. (1998). The IQGAP-related protein DGAP1 interacts with Rac and is involved in the modulation of the F-actin cytoskeleton and control of cell motility. *J. Cell Sci.* **111**, 3059-3071.

Faix, J., Steinmetz, M., Boves, H., Kammerer, R. A., Lottspeich, F., Mintert, U., Murphy, J., Stock, A., Aebi, U. and Gerisch, G. (1996). Cortexillins, major determinants of cell shape and size, are actin-bundling proteins with a parallel coiled-coil tail. *Cell* **86**, 631-642.

Faix, J., Weber, I., Mintert, U., Kohler, J., Lottspeich, F. and Marriott, G. (2001). Recruitment of cortexillin into the cleavage furrow is controlled by Rac1 and IQGAP-related proteins. *EMBO J.* **20**, 3705-3715.

Galkin, V. E., Orlova, A. and Egelman, E. H. (2012). Actin filaments as tension sensors. *Curr. Biol.* **22**, R96-R101.

Gardel, M. L., Shin, J. H., MacKintosh, F. C., Mahadevan, L., Matsudaira, P. and Weitz, D. A. (2004). Elastic behavior of cross-linked and bundled actin networks. *Science* **304**, 1301-1305.

Girard, K. D., Kuo, S. C. and Robinson, D. N. (2006). *Dictyostelium* myosin-II mechanochemistry promotes active behavior of the cortex on long time-scales. *Proc. Natl. Acad. Sci. USA* **103**, 2103-2108.

Goldmann, W. H. and Isenberg, G. (1993). Analysis of filamin and alpha-actinin binding to actin by the stopped flow method. *FEBS Lett.* **336**, 408-410.

Guilak, F., Cohen, D. M., Estes, B. T., Gimble, J. M., Liedtke, W. and Chen, C. S. (2009). Control of stem cell fate by physical interactions with the extracellular matrix. *Cell Stem Cell* **5**, 17-26.

- Guo, M., Ehrlicher, A. J., Jensen, M. H., Renz, M., Moore, J. R., Goldman, R. D., Lippincott-Schwartz, J., Mackintosh, F. C. and Weitz, D. A.** (2014). Probing the stochastic, motor-driven properties of the cytoplasm using force spectrum microscopy. *Cell* **158**, 822-832.
- Hamann, J. C., Surcel, A., Chen, R., Teragawa, C., Albeck, J. G., Robinson, D. N. and Overholtzer, M.** (2017). Entosis Is Induced by Glucose Starvation. *Cell Rep.* **20**, 201-210.
- Hatch, A. L., Gurel, P. S. and Higgs, H. N.** (2014). Novel roles for actin in mitochondrial fission. *J. Cell Sci.* **127**, 4549-4560.
- Henty-Ridilla, J. L., Rankova, A., Eskin, J. A., Kenny, K. and Goode, B. L.** (2016). Accelerated actin filament polymerization from microtubule plus ends. *Science* **352**, 1004-1009.
- Hergovich, A. and Hemmings, B. A.** (2012). Hippo signalling in the G2/M cell cycle phase: lessons learned from the yeast MEN and SIN pathways. *Semin. Cell Dev. Biol.* **23**, 794-802.
- Horton, E. R., Humphries, J. D., James, J., Jones, M. C., Askari, J. A. and Humphries, M. J.** (2016). The integrin adhesome network at a glance. *J. Cell Sci.* **129**, 4159-4163.
- Huber, F., Boire, A., Lopez, M. P. and Koenderink, G. H.** (2015). Cytoskeletal crosstalk: when three different personalities team up. *Curr. Opin. Cell Biol.* **32**, 39-47.
- Husbands, A. Y., Aggarwal, V., Ha, T. and Timmermans, M. C.** (2016). In Planta Single-Molecule Pull-Down Reveals Tetrameric Stoichiometry of HD-ZIPIII:LITTLE ZIPPER Complexes. *Plant Cell* **28**, 1783-1794.
- Jacobson, K., Derzko, Z., Wu, E. S., Hou, Y. and Poste, G.** (1976). Measurement of the lateral mobility of cell surface components in single, living cells by fluorescence recovery after photobleaching. *J. Supramol. Struct.* **5**, 565(417)-576(428).
- Jain, A., Liu, R., Ramani, B., Arauz, E., Ishitsuka, Y., Raganathan, K., Park, J., Chen, J., Xiang, Y. K. and Ha, T.** (2011). Probing cellular protein complexes using single-molecule pull-down. *Nature* **473**, 484-488.
- Kaczmarek, Z., Ortega, E., Goudarzi, A., Huang, H., Kim, S., Marquez, J. A., Zhao, Y., Khochbin, S. and Panne, D.** (2017). Structure of p300 in complex with acyl-CoA variants. *Nat. Chem. Biol.* **13**, 21-29.
- Kassianidou, E., Kalita, J. and Lim, R. Y. H.** (2019). The role of nucleocytoplasmic transport in mechanotransduction. *Exp. Cell Res.* **377**, 86-93.
- Kee, Y. S., Ren, Y., Dorfman, D., Iijima, M., Firtel, R., Iglesias, P. A. and Robinson, D. N.** (2012). A mechanosensory system governs myosin II accumulation in dividing cells. *Mol. Biol. Cell* **23**, 1510-23.

Kim, J. H., Ren, Y., Ng, W. P., Li, S., Son, S., Kee, Y. S., Zhang, S., Zhang, G., Fletcher, D. A., Robinson, D. N. et al. (2015). Mechanical tension drives cell membrane fusion. *Dev. Cell* **32**, 561-573.

Kothari, P., Johnson, C., Sandone, C., Iglesias, P. A. and Robinson, D. N. (2019a). How the mechanobiome drives cell behavior, viewed through the lens of control theory. *J. Cell Sci.* **132**.

Kothari, P., Schiffhauer, E. S. and Robinson, D. N. (2017). Cytokinesis from nanometers to micrometers and microseconds to minutes. *Methods Cell Biol.* **137**, 307-322.

Kothari, P., Srivastava, V., Aggarwal, V., Tchernyshyov, I., Van Eyk, J. E., Ha, T. and Robinson, D. N. (2019b). Contractility kits promote assembly of the mechanoresponsive cytoskeletal network. *J. Cell Sci.* **132**, 1-12.

Kovacs, M., Thirumurugan, K., Knight, P. J. and Sellers, J. R. (2007). Load-dependent mechanism of nonmuscle myosin 2. *Proc. Natl. Acad. Sci. USA* **104**, 9994-9999.

Laplace, C., Huang, F., Tebbs, I. R., Bewersdorf, J. and Pollard, T. D. (2016). Molecular organization of cytokinesis nodes and contractile rings by super-resolution fluorescence microscopy of live fission yeast. *Proc. Natl. Acad. Sci. USA* **113**, E5876-E5885.

Laporte, D., Coffman, V. C., Lee, I. J. and Wu, J. Q. (2011). Assembly and architecture of precursor nodes during fission yeast cytokinesis. *J. Cell Biol.* **192**, 1005-1021.

Lee, S., Shen, Z., Robinson, D. N., Briggs, S. and Firtel, R. A. (2010). Involvement of the cytoskeleton in controlling leading-edge function during chemotaxis. *Mol. Biol. Cell* **21**, 1810-1824.

Lian, I., Kim, J., Okazawa, H., Zhao, J., Zhao, B., Yu, J., Chinnaiyan, A., Israel, M. A., Goldstein, L. S., Abujarour, R. et al. (2010). The role of YAP transcription coactivator in regulating stem cell self-renewal and differentiation. *Genes Dev.* **24**, 1106-1118.

Lippincott-Schwartz, J., Snapp, E. and Kenworthy, A. (2001). Studying protein dynamics in living cells. *Nat. Rev. Mol. Cell Biol.* **2**, 444-56.

Liu, B., Lin, Y., Darwanto, A., Song, X., Xu, G. and Zhang, K. (2009). Identification and characterization of propionylation at histone H3 lysine 23 in mammalian cells. *J. Biol. Chem.* **284**, 32288-95.

Luo, T., Mohan, K., Iglesias, P. A. and Robinson, D. N. (2013). Molecular mechanisms of cellular mechanosensing. *Nat. Mater.* **12**, 1064-1071.

Luo, T., Mohan, K., Srivastava, V., Ren, Y., Iglesias, P. A. and Robinson, D. N. (2012). Understanding the cooperative interaction between myosin II and actin

crosslinkers mediated by actin filaments during mechanosensation. *Biophys. J.* **102**, 238-247.

Luo, T. and Robinson, D. N. (2015). Kinetic Monte Carlo simulations of the assembly of filamentous biomacromolecules by dimer addition mechanism. *RSC Adv* **5**, 3922-3929.

Luo, T., Srivastava, V., Ren, Y. and Robinson, D. N. (2014). Mimicking the mechanical properties of the cell cortex by the self-assembly of an actin cortex in vesicles. *Appl. Phys. Lett.* **104**, 153701-153705.

Mahajan, R. K. and Pardee, J. D. (1996). Assembly mechanism of *Dictyostelium* myosin II: Regulation by K^+ , Mg^{2+} , and actin filaments. *Biochemistry* **35**, 15504-15514.

Mahajan, R. K., Vaughan, K. T., Johns, J. A. and Pardee, J. D. (1989). Actin filaments mediate *Dictyostelium* myosin assembly in vitro. *Proc. Natl. Acad. Sci. USA* **86**, 6161-6165.

Manukyan, A., Ludwig, K., Sanchez-Manchinelly, S., Parsons, S. J. and Stukenberg, P. T. (2015). A complex of p190RhoGAP-A and anillin modulates RhoA-GTP and the cytokinetic furrow in human cells. *J. Cell Sci.* **128**, 50-60.

Martin, S. G. and Berthelot-Grosjean, M. (2009). Polar gradients of the DYRK-family kinase Pom1 couple cell length with the cell cycle. *Nature* **459**, 852-6.

Mason, D. E., Collins, J. M., Dawahare, J. H., Nguyen, T. D., Lin, Y., Voytik-Harbin, S. L., Zorlutuna, P., Yoder, M. C. and Boerckel, J. D. (2019). YAP and TAZ limit cytoskeletal and focal adhesion maturation to enable persistent cell motility. *J. Cell Biol.* **218**, 1369-1389.

Miao, Y., Bhattacharya, S., Edwards, M., Cai, H., Inoue, T., Iglesias, P. A. and Devreotes, P. N. (2017). Altering the threshold of an excitable signal transduction network changes cell migratory modes. *Nat. Cell Biol.* **19**, 329-340.

Moeendarbary, E. and Harris, A. R. (2014). Cell mechanics: principles, practices, and prospects. *Wiley Interdiscip. Rev. Syst. Biol. Med.* **6**, 371-88.

Mohan, K., Luo, T., Robinson, D. N. and Iglesias, P. A. (2015). Cell shape regulation through mechanosensory feedback control. *Journal of The Royal Society Interface* **12**.

Mondal, S., Burgute, B., Rieger, D., Muller, R., Rivero, F., Faix, J., Schleicher, M. and Noegel, A. A. (2010). Regulation of the actin cytoskeleton by an interaction of IQGAP related protein GAPA with filamin and cortexillin I. *PLoS One* **5**, e15440.

Moseley, J. B., Mayeux, A., Paoletti, A. and Nurse, P. (2009). A spatial gradient coordinates cell size and mitotic entry in fission yeast. *Nature* **459**, 857-60.

Mukhina, S., Wang, Y. L. and Murata-Hori, M. (2007). Alpha-actinin is required for tightly regulated remodeling of the actin cortical network during cytokinesis. *Dev. Cell* **13**, 554-565.

Munjal, A., Philippe, J. M., Munro, E. and Lecuit, T. (2015). A self-organized biomechanical network drives shape changes during tissue morphogenesis. *Nature* **524**, 351-355.

Naganathan, S. R., Furthauer, S., Rodriguez, J., Fievet, B. T., Julicher, F., Ahringer, J., Cannistraci, C. V. and Grill, S. W. (2018). Morphogenetic degeneracies in the actomyosin cortex. *Elife* **7**, 1-21.

Nagy, A., Takagi, Y., Billington, N., Sun, S. A., Hong, D. K., Homsher, E., Wang, A. and Sellers, J. R. (2013). Kinetic characterization of nonmuscle myosin IIb at the single molecule level. *J. Biol. Chem.* **288**, 709-722.

Ngo, T., Miao, X., Robinson, D. N. and Zhou, Q. Q. (2016). An RNA-binding protein, RNP-1, protects microtubules from nocodazole and localizes to the leading edge during cytokinesis and cell migration in Dictyostelium cells. *Acta Pharmacol. Sin.* **37**, 1449-1457.

Overholtzer, M., Mailleux, A. A., Mouneimne, G., Normand, G., Schnitt, S. J., King, R. W., Cibas, E. S. and Brugge, J. S. (2007). A nonapoptotic cell death process, entosis, that occurs by cell-in-cell invasion. *Cell* **131**, 966-979.

Pancier, T., Azzolin, L., Cordenonsi, M. and Piccolo, S. (2017). Mechanobiology of YAP and TAZ in physiology and disease. *Nat. Rev. Mol. Cell Biol.* **18**, 758-770.

Pegoraro, A. F., Janmey, P. and Weitz, D. A. (2017). Mechanical Properties of the Cytoskeleton and Cells. *Cold Spring Harb. Perspect. Biol.* **9**, 1-12.

Peltz, G., Spudich, J. A. and Parham, P. (1985). Monoclonal antibodies against seven sites on the head and tail of Dictyostelium myosin. *J. Cell Biol.* **100**, 1016-1023.

Picariello, H. S., Kenchappa, R. S., Rai, V., Crish, J. F., Dovas, A., Pogoda, K., McMahon, M., Bell, E. S., Chandrasekharan, U., Luu, A. et al. (2019). Myosin IIA suppresses glioblastoma development in a mechanically sensitive manner. *Proc Natl Acad Sci U S A*.

Poirier, C. C., Ng, W. P., Robinson, D. N. and Iglesias, P. A. (2012). Deconvolution of the cellular force-generating subsystems that govern cytokinesis furrow ingression. *PLoS Comput. Biol.* **8**, e1002467.

Reichl, E. M., Ren, Y., Morphew, M. K., Delannoy, M., Effler, J. C., Girard, K. D., Divi, S., Iglesias, P. A., Kuo, S. C. and Robinson, D. N. (2008a). Interactions between myosin and actin crosslinkers control cytokinesis contractility dynamics and mechanics. *Curr. Biol.* **18**, 471-480.

Reichl, E. M., Ren, Y., Morphew, M. K., Delannoy, M., Effler, J. C., Girard, K. D., Divi, S., Iglesias, P. A., Kuo, S. C. and Robinson, D. N. (2008b). Interactions between myosin and actin crosslinkers control cytokinesis contractility dynamics and mechanics. *Curr. Biol.* **18**, 471-480.

Ren, Y., Effler, J. C., Norstrom, M., Luo, T., Firtel, R. A., Iglesias, P. A., Rock, R. S. and Robinson, D. N. (2009). Mechanosensing through Cooperative Interactions between Myosin II and the Actin Crosslinker Cortexillin I. *Curr. Biol.* **19**, 1421-1428.

Ren, Y., West-Foyle, H., Surcel, A., Miller, C. and Robinson, D. N. (2014). Genetic suppression of a phosphomimic myosin II identifies system-level factors that promote myosin II cleavage furrow accumulation. *Mol. Biol. Cell* **25**, 4150-4165.

Robinson, D. N., Kee, Y.-S., Luo, T. and Surcel, A. (2012). Understanding how dividing cells change shape. In *The Comprehensive Biophysics*, vol. 7 (ed. E. H. Egelman), pp. 48-72: Elsevier.

Robinson, D. N. and Spudich, J. A. (2000). Dynacortin, a Genetic Link between Equatorial Contractility and Global Shape Control Discovered by Library Complementation of a Dictyostelium discoideum Cytokinesis Mutant. *J. Cell Biol.* **150**, 823-838.

Ruppel, K. M., Uyeda, T. Q. and Spudich, J. A. (1994). Role of highly conserved lysine 130 of myosin motor domain. In vivo and in vitro characterization of site specifically mutated myosin. *J. Biol. Chem.* **269**, 18773-18780.

Salvi, A. M. and DeMali, K. A. (2018). Mechanisms linking mechanotransduction and cell metabolism. *Curr. Opin. Cell Biol.* **54**, 114-120.

Samant, S. A., Pillai, V. B., Sundaresan, N. R., Shroff, S. G. and Gupta, M. P. (2015). Histone Deacetylase 3 (HDAC3)-dependent Reversible Lysine Acetylation of Cardiac Myosin Heavy Chain Isoforms Modulates Their Enzymatic and Motor Activity. *J. Biol. Chem.* **290**, 15559-69.

Schiffhauer, E. S., Luo, T., Mohan, K., Srivastava, V., Qian, X., Griffis, E. R., Iglesias, P. A. and Robinson, D. N. (2016). Mechanoaccumulative Elements of the Mammalian Actin Cytoskeleton. *Curr. Biol.* **26**, 1473-1479.

Schiffhauer, E. S., Ren, Y., Iglesias, V. A., Kothari, P., Iglesias, P. A. and Robinson, D. N. (2019). Myosin IIB assembly state determines its mechanosensitive dynamics. *J. Cell Biol.* **218**, 895-908.

Schiffhauer, E. S. and Robinson, D. N. (2017). Mechanochemical Signaling Directs Cell-Shape Change. *Biophys. J.* **112**, 207-214.

Shutova, M. S., Asokan, S. B., Talwar, S., Assoian, R. K., Bear, J. E. and Svitkina, T. M. (2017). Self-sorting of nonmuscle myosins IIA and IIB polarizes the cytoskeleton and modulates cell motility. *J. Cell Biol.* **216**, 2877-2889.

Simanis, V. (2015). Pombe's thirteen - control of fission yeast cell division by the septation initiation network. *J. Cell Sci.* **128**, 1465-74.

Smith, L., Cho, S. and Discher, D. E. (2017). Mechanosensing of matrix by stem cells: From matrix heterogeneity, contractility, and the nucleus in pore-migration to cardiogenesis and muscle stem cells in vivo. *Semin. Cell Dev. Biol.* **71**, 84-98.

Srivastava, V., Iglesias, P. A. and Robinson, D. N. (2016). Cytokinesis: Robust cell shape regulation. *Semin. Cell Dev. Biol.* **53**, 39-44.

Srivastava, V. and Robinson, D. N. (2015). Mechanical stress and network structure drive protein dynamics during cytokinesis. *Curr. Biol.* **25**, 663-670.

Straight, A. F., Field, C. M. and Mitchison, T. J. (2005). Anillin binds nonmuscle myosin II and regulates the contractile ring. *Mol. Biol. Cell* **16**, 193-201.

Sun, Q., Luo, T., Ren, Y., Florey, O., Shirasawa, S., Sasazuki, T., Robinson, D. N. and Overholtzer, M. (2014). Competition between human cells by entosis. *Cell Res.* **24**, 1299-1310.

Sun, Z., Costell, M. and Fassler, R. (2019). Integrin activation by talin, kindlin and mechanical forces. *Nat. Cell Biol.* **21**, 25-31.

Surcel, A., Ng, W. P., West-Foyle, H., Zhu, Q., Ren, Y., Avery, L. B., Krenc, A. K., Meyers, D. J., Rock, R. S., Anders, R. A. et al. (2015). Pharmacological activation of myosin II paralogs to correct cell mechanics defects. *Proc. Natl. Acad. Sci. USA* **112**, 1428-1433.

Surcel, A. and Robinson, D. N. (2019). Meddling with myosin's mechanobiology in cancer. *Proc Natl Acad Sci U S A.*

Surcel, A., Schiffhauer, E. S., Thomas, D. G., Zhu, Q., DiNapoli, K. T., Herbig, M., Otto, O., West-Foyle, H., Jacobi, A., Krater, M. et al. (2019). Targeting mechanoresponsive proteins in pancreatic cancer: 4-hydroxyacetophenone blocks dissemination and invasion by activating MYH14. *Cancer Res.*

Tharp, K. M., Kang, M. S., Timblin, G. A., Dempersmier, J., Dempsey, G. E., Zushin, P. H., Benavides, J., Choi, C., Li, C. X., Jha, A. K. et al. (2018). Actomyosin-Mediated Tension Orchestrates Uncoupled Respiration in Adipose Tissues. *Cell Metab.* **27**, 602-615 e4.

Tokuraku, K., Kurogi, R., Toya, R. and Uyeda, T. Q. P. (2009). Novel mode of cooperative binding between myosin and Mg²⁺-actin filaments in the presence of low concentrations of ATP. *J. Mol. Biol.* **386**, 149-162.

Totaro, A., Castellan, M., Battilana, G., Zanconato, F., Azzolin, L., Giulitti, S., Cordenonsi, M. and Piccolo, S. (2017). YAP/TAZ link cell mechanics to Notch signalling to control epidermal stem cell fate. *Nat. Commun.* **8**, 15206-15219.

Uyeda, T. Q., Iwadate, Y., Umeki, N., Nagasaki, A. and Yumura, S. (2011). Stretching actin filaments within cells enhances their affinity for the myosin II motor domain. *PLoS One* **6**, e26200.

Vavylonis, D., Wu, J. Q., Hao, S., O'Shaughnessy, B. and Pollard, T. D. (2008). Assembly mechanism of the contractile ring for cytokinesis by fission yeast. *Science* **319**, 97-100.

- Veigel, C., Molloy, J. E., Schmitz, S. and Kendrick-Jones, J.** (2003). Load-dependent kinetics of force production by smooth muscle myosin measured with optical tweezers. *Nat. Cell Biol.* **5**, 980-6.
- Weissbach, L., Bernards, A. and Herion, D. W.** (1998). Binding of myosin essential light chain to the cytoskeleton-associated protein IQGAP1. *Biochem. Biophys. Res. Commun.* **251**, 269-276.
- West-Foyle, H., Kothari, P., Osborne, J. and Robinson, D. N.** (2018). 14-3-3 proteins tune non-muscle myosin II assembly. *J. Biol. Chem.* **293**, 6751-6761.
- White, C. D., Brown, M. D. and Sacks, D. B.** (2009). IQGAPs in cancer: a family of scaffold proteins underlying tumorigenesis. *FEBS Lett.* **583**, 1817-24.
- Wong, S. Y., Ulrich, T. A., Deleyrolle, L. P., MacKay, J. L., Lin, J. M., Martuscello, R. T., Jundi, M. A., Reynolds, B. A. and Kumar, S.** (2015). Constitutive activation of myosin-dependent contractility sensitizes glioma tumor-initiating cells to mechanical inputs and reduces tissue invasion. *Cancer Res.* **75**, 1113-22.
- Wu, J. Q. and Pollard, T. D.** (2005). Counting cytokinesis proteins globally and locally in fission yeast. *Science* **310**, 310-314.
- Wu, X., Kodama, A. and Fuchs, E.** (2008). ACF7 regulates cytoskeletal-focal adhesion dynamics and migration and has ATPase activity. *Cell* **135**, 137-148.
- Yabuta, N., Okada, N., Ito, A., Hosomi, T., Nishihara, S., Sasayama, Y., Fujimori, A., Okuzaki, D., Zhao, H., Ikawa, M. et al.** (2007). Lats2 is an essential mitotic regulator required for the coordination of cell division. *J. Biol. Chem.* **282**, 19259-71.
- Yap, A. S., Duszyc, K. and Viasnoff, V.** (2018). Mechanosensing and Mechanotransduction at Cell-Cell Junctions. *Cold Spring Harb. Perspect. Biol.* **10**.
- Zaidel-Bar, R., Zhenhuan, G. and Luxenburg, C.** (2015). The contractome--a systems view of actomyosin contractility in non-muscle cells. *J. Cell Sci.* **128**, 2209-2217.
- Zhang, W. and Robinson, D. N.** (2005). Balance of actively generated contractile and resistive forces controls cytokinesis dynamics. *Proc. Natl. Acad. Sci. USA* **102**, 7186-7191.
- Zhou, Q., Kee, Y. S., Poirier, C. C., Jelinek, C., Osborne, J., Divi, S., Surcel, A., Will, M. E., Eggert, U. S., Muller-Taubenberger, A. et al.** (2010). 14-3-3 coordinates microtubules, Rac, and myosin II to control cell mechanics and cytokinesis. *Curr. Biol.* **20**, 1881-1889.

Curriculum Vitae

Priyanka Kothari

725 N Wolfe St, Physiology 100, Baltimore, Maryland 21205 | 732-284-8918 |
pkothar6@jhmi.edu

EDUCATION

Ph.D. in Cell Biology Johns Hopkins University School of Medicine, Baltimore, MD	January 2020
M.S. in Chemistry University of Pennsylvania, Philadelphia, MD	May 2014
B.A. in Biochemistry , <i>cum laude</i> , with distinction University of Pennsylvania, Philadelphia, MD	May 2014

RESEARCH EXPERIENCE

Ph.D. Candidate , Johns Hopkins School of Medicine Biochemistry, Cellular, and Molecular Biology Program Principal Investigator: Douglas N. Robinson, Ph.D. Dissertation: Deciphering the Biochemical Interactions of the Mechanoresponsive Contractility Controller	2014-2020
Research Associate , University of Pennsylvania Department of Biology Principal Investigator: Michael A. Lampson, Ph.D. Master's Thesis: Mechanical Regulation of the Mitotic Wavefront in Zebrafish Embryos	2011-2014

SCHOLARSHIPS AND FELLOWSHIPS

PEO Chapter K Merit Scholar Award	2019
Kirschstein National Research Service Award F31	2018
Lewis Travel Award, Department of Cell Biology	2017
Thomas Wilson Graduate Fellowship, mentor for summer outreach program	2016
Hopkins Graduate Students Association Travel Award	2016

ACADEMIC AND RESEARCH AWARDS

David Yue Hopkins Young Investigator Day Award	2019
Honorable Mention Presentation at Biogen Drug Development Conference	2018
2 nd Place Poster Award, Women in STEM Symposium	2018
University of Pennsylvania University Scholars Research Grant	2013

PUBLICATIONS

Kothari P, Johnson C, Sandone C, Iglesias PA, Robinson DN (2019) How the mechanobiome drives cell behavior, viewed through the lens of control theory. *Journal of Cell Science*, 132(17):jcs234476. PMID: PMC6771144

Schiffhauer ES, Ren Y, Iglesias V, **Kothari, P**, Iglesias PA, Robinson DN (2019) Myosin IIB assembly-state determines myosin IIB mechanosensitive dynamics. *Journal of Cell Biology*, 218(3):895-908. PMID: PMC6400566

Kothari P, Srivastava V, Aggarwal V, Tchernyshyov I, Van Eyk JE, Ha T, and Robinson DN (2018) Contractility kits promote assembly of the mechanoresponsive cytoskeletal network. *Journal of Cell Science*, 132(2):jcs226704. (Cover article; associated First person interview published in the same issue). PMID: PMC6362397

West-Foyle, H, **Kothari, P**, Osborne, J, Robinson, DN (2018) 14-3-3 proteins tune non-muscle myosin II assembly. *Journal of Biological Chemistry*. 293(18), 6751-6761. PMID: PMC5936829

Kothari, P, Schiffhauer, ES, and Robinson, DN (2017) Cytokinesis from nanometers to micrometers and microseconds to minutes. In Arnaud Echard (ed.) *Methods in Cell Biology*. Elsevier, 137:307-322.

Zhang M, **Kothari P**, Lampson MA (2015) Spindle assembly checkpoint acquisition at the mid-blastula transition. *PLOS ONE*, 10(3): e0119285. PMID: PMC4351100

Zhang M, **Kothari P**, Mullins M, Lampson MA (2014) Regulation of zygotic genome activation and DNA damage checkpoint acquisition at the mid-blastula transition. *Cell Cycle*, 13: 3828-38. PMID: PMC4614548

RESEARCH PRESENTATIONS

Oral Presentations

Mechanobiology Subgroup, Biophysical Society Annual Meeting	2018
Biochemistry, Cellular and Molecular Biology Graduate Program Retreat	2017
Cytokinesis Subgroup, American Society for Cell Biology	2016
Cell Mechanics Platform Presentation, Biophysical Society Annual Meeting	2016
Center for Cell Dynamics Seminar, Johns Hopkins School of Medicine	2016

Poster Presentations

Discovery on Target Annual Meeting	2019
Biophysical Society Annual Meeting	2018, 2019
Women in STEM Symposium	2018
Motile and Contractile Systems Gordon Conference	2017
University of Maryland Biophysics Symposium	2017
American Society for Cell Biology	2016, 2017

SERVICE AND LEADERSHIP

Mentor	2014-present
Thread, Baltimore, MD	
Proposal Writing Workshop Mentor	2018
JHMI, Baltimore, MD	
Graduate Student Recruitment Coordinator	2016-2017
Biochemistry, Cellular, and Molecular Biology Program, JHMI, Baltimore, MD	
Instructor and Mentor	2015, 2016
Summer Academic Research Experience, JHMI, Baltimore, MD	

PROFESSIONAL MEMBERSHIPS

Women In Bio	2019-present
American Society for Cell Biology	2015-present
Biophysical Society	2015-present